

Short-term and long-term tremor migration patterns of the Cascadia 2004 tremor and slow slip episode using small aperture seismic arrays

Wendy A. McCausland,¹ Kenneth C. Creager,² Mario La Rocca,³ and Stephen D. Malone²

Received 1 September 2008; revised 5 February 2010; accepted 26 March 2010; published 25 August 2010.

[1] Tectonic tremor has been recorded at many subduction zones, including the Nankai, Cascadia, Mexican, and Alaskan subduction zones. This study, the first to use small aperture seismic arrays to track tremor, deployed three small aperture seismic arrays along the Cascadia subduction zone during a tremor and slow slip episode in July 2004. The tremor was active during virtually all (up to 99%) minutes of the analyzed tremor episode using 5 min sample windows. Individual wave phases were tracked across the arrays and used to derive slowness vectors. These were compared with slowness vectors computed from a standard layered Earth model to derive tremor locations. Locations were stable within a volume roughly 250 km² in epicenter and 20 km in depth for hours to days before moving to a new volume. The migration between volumes was not smooth, and the movement of the sources within the volume followed no specific pattern. Overall migration speeds along the strike of the subduction zone were between 5 and 15 km/d; smaller scale migration speeds between volumes reached speeds up to 2 km/min. Uncertainties in the best locations were 5 km in epicenter and 10 km in depth. For this data set and processing methodology, tremor does not locate predominately on the primary subduction interface. Our favored model for the generation of tectonic tremor signals is that the tremor is triggered by stress and fluid pressure changes caused by slow slip and is composed, at least in part, of low-frequency earthquakes broadly distributed in location.

Citation: McCausland, W. A., K. C. Creager, M. La Rocca, and S. D. Malone (2010), Short-term and long-term tremor migration patterns of the Cascadia 2004 tremor and slow slip episode using small aperture seismic arrays, *J. Geophys. Res.*, 115, B00A24, doi:10.1029/2008JB006063.

1. Introduction

[2] Where and how the stresses created by subduction are released is important to the assessment of seismic hazards. The rate of plate convergence can be estimated using long-term GPS measurements [e.g., *Dragert et al.*, 2001; *Miller et al.*, 2002] and borehole tiltmeters [*Hirose and Obara*, 2005]. In Cascadia and elsewhere that process is not smooth, rather there are periodic, local reversals to the steady convergent plate motion called slow slip events [*Dragert et al.*, 2001; *Miller et al.*, 2002]. In the northern Cascadia subduction zone, the slow slip events are accompanied by seismic tremor and occur at regular intervals of 14 ± 2 months [*Miller et al.*, 2002]. This seismic tremor (herein called tectonic tremor) has been detected at a multitude of subduction zones worldwide [*Obara*, 2002; *Schwartz*

and *Rokosky*, 2007], notably in Cascadia [e.g., *Rogers and Dragert*, 2003; *McCausland et al.*, 2005; *Szeliga et al.*, 2004] and along sections of the transform boundary of the San Andreas Fault system [*Nadeau and Dolenc*, 2005]. Yet the two phenomena apparently do not always occur together: to date no tectonic tremor has been observed associated with slow slip events in New Zealand [e.g., *Douglas et al.*, 2005; *Wallace and Beavan*, 2006], or Hawaii [*Segall et al.*, 2006; *Brooks et al.*, 2006], and no slow slip has been observed in Parkfield associated with tectonic tremor. Even in subduction zones, there are episodes of tectonic tremor that have no accompanying detectable slow slip [e.g., *McCausland et al.*, 2005], though this may be due to the limits of GPS resolution. A third phenomenon called very low frequency earthquakes (VLF), thus far only detected in southwest Japan, are sometimes coincident with tectonic tremor [e.g., *Ito et al.*, 2007].

[3] In Cascadia tectonic tremor signals are emergent, occur as bursts that last for minutes to hours (Figure 1), have a dominant frequency content between 1 and 10 Hz, large horizontal component amplitudes, and apparent velocities (network-scale moveout of tremor burst) around 4 km/s. Waveforms cannot be directly correlated between stations separated by more than a few kilometers (Figure 1). These

¹U.S. Geological Survey, Cascades Volcano Observatory, Vancouver, Washington, USA.

²Department of Earth and Space Sciences, University of Washington, Seattle, Washington, USA.

³Istituto Nazionale di Geofisica e Vulcanologia, Osservatorio Vesuviano, Naples, Italy.

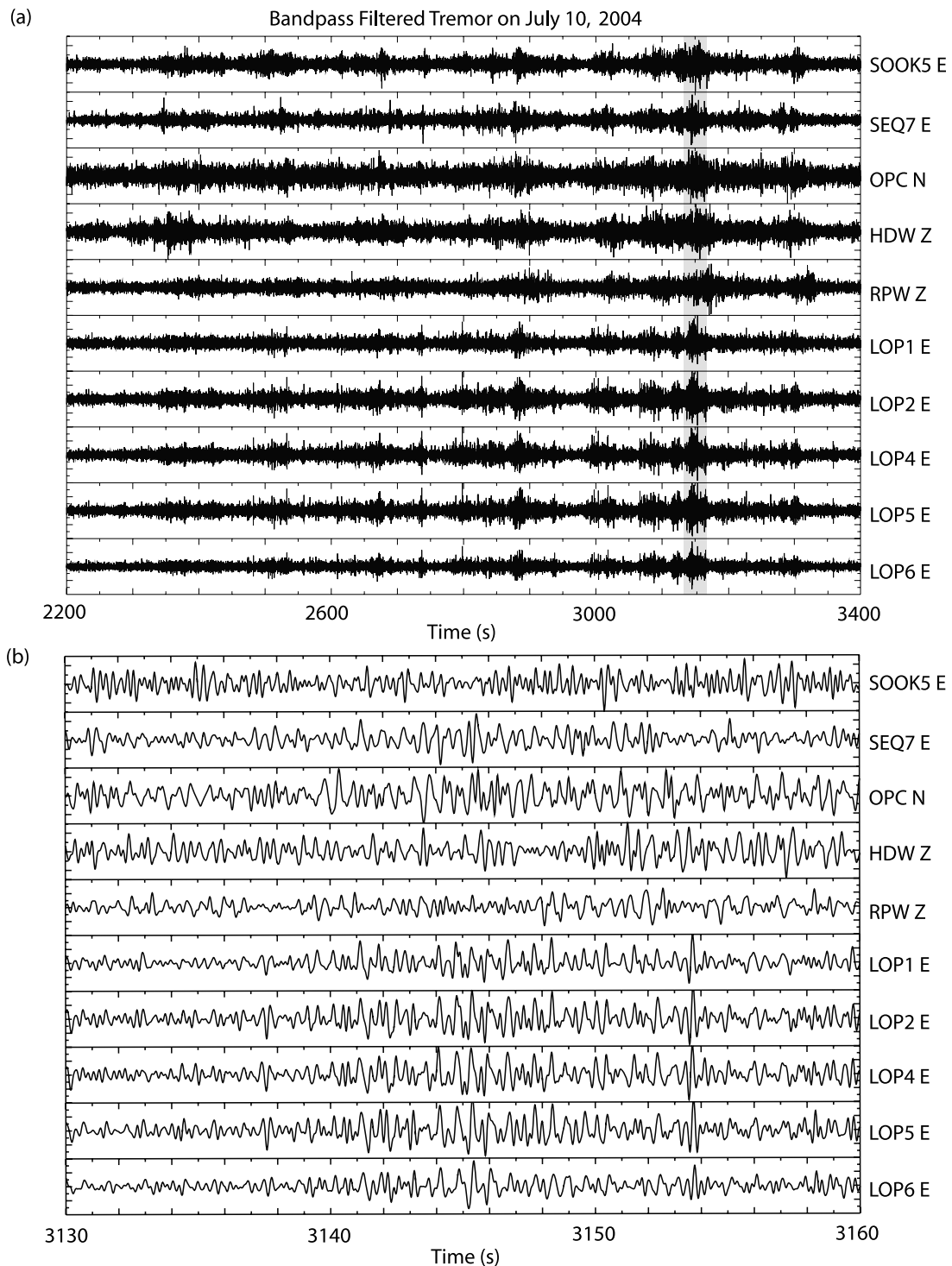


Figure 1. Band-pass-filtered tremor data on five broadly distributed network stations (top five traces) and on five stations from the Lopez small aperture array (bottom five traces). (a) The 20 min of data on 10 July 2004, where bursts can be identified and tracked across network stations. (b) The 30 s of data from the highlighted section of Figure 1a. On the network stations the individual phases cannot be tracked between stations, but on the array the signals are highly correlated and individual phases can be identified across all stations.

characteristics make it difficult to use traditional network data and processing techniques to locate the source of the signals.

[4] Previous studies of tectonic tremor have used regional seismic networks to locate and detect tremor using three methods. The first uses relative arrival times at network stations obtained from amplitude variations that can be tracked between network stations by the cross-correlation of signal envelopes (band-pass filtered, rectified signals, herein called envelopes) [Obara, 2002; McCausland *et al.*, 2005]. This method is unable to precisely determine the depth of the events because the tremor signals lack phases that can be tracked from regional station to regional station. The second method is the source scanning algorithm (SSA), which searches all space for bright spots of energy (sources) [Kao and Shan, 2004; Kao *et al.*, 2005, 2006]. This method is computationally intensive and results depend on the identification of amplitude variations that are common to many stations. Both these methods assume that the peaks in the tremor signal represent the direct, minimum-time arrivals such as S waves. Because the envelopes are maximum amplitude, this assumption may not be valid. The third method cross-correlates previously identified and located low frequency earthquakes on or near the subduction zone interface with the tremor signals [Shelly *et al.*, 2006]. However, there is no catalog of independently occurring, network-detected low frequency earthquakes in Cascadia.

[5] Studies using the first two methods in Cascadia have shown that the hypocentral locations of tremor have a wide depth distribution (12–60 km) with errors on the order of kilometers in epicenter and 10 km in depth [Kao *et al.*, 2005; McCausland *et al.*, 2005; Kao *et al.*, 2006]. The distribution is not just a wider zone whose geometry mimics the subducting slab, and the spread in depths is much greater than the errors. This is in strong contrast to Japan, where low frequency earthquakes occur concurrently with tremor and locate along and just above the subducting slab interface (third method [Shelly *et al.*, 2006]). However, only low frequency earthquakes located on the plate interface were used as template events, potentially biasing the results. Furthermore, it has not yet been proven that these low frequency events explain the entire tremor wavefield.

[6] The signals of tectonic tremor in Cascadia are dominated by SH wave phases, but there is evidence of weak P wave phases when the data are analyzed on small aperture seismic arrays [La Rocca *et al.*, 2005, 2010]. This led to the development of a fourth method that identifies P and S wave phases within the tremor signal, and then uses the S-P time to locate the source. The use of the T_{s-p} time poses a strong constraint on the source location, reducing dramatically the uncertainty in the source depth. Many P-S wave sequences have been identified in the July 2004 tremor, however as with method 3, the sources identified do not account for all the recorded tremor wavefield. Results obtained by this method indicate that most of sources are much closer to the subducting slab interface (within ± 8 km) than methods 1 and 2 suggest, but, again, not on a plane that simply mirrors the shape of the interface [La Rocca *et al.*, 2009, 2010]. All these studies have not yet led to definitive models of the mechanics of tremor sources and their relationship to slow slip. More importantly for hazard, the connections between

tremor, slow slip and the potential for great earthquakes in the locked portions of plate boundaries remains unclear.

[7] In northern Cascadia, network data show the net migration of tremor (along the strike of the subduction zone) at speeds between 5 and 12 km/d [Kao *et al.*, 2006]. However, network data alone are not adequate to understand how deep tremor changes and progresses on much shorter timescales (seconds to minutes), which could be more directly related with the source process. Thus another approach to studying tremor location, the approach taken in the present study, is to deploy arrays of seismometers and use array processing techniques such that the entire tremor waveform can be correlated among stations that are close to each other to define a coherent wavefront (Figure 1). Array processing techniques can then be used to determine the apparent velocity and back-azimuth of the signal wavefronts. This experiment is the first to use small aperture seismic arrays to study the wave properties of and spatial and temporal changes of tectonic tremor. Subsequent tectonic tremor array designs, locations and processing techniques in Cascadia utilized the experience of this work [e.g., Wech and Creager, 2007].

[8] We installed three temporary seismic arrays in March and April 2004 to study tectonic tremor associated with one tremor and slow slip episode that occurred in July 2004 in the northern section of the Cascadia subduction zone. At each array we determined the apparent slowness and back-azimuth of the tremor in 5 min and 30 s windows throughout the sequence of tremor (section 2.2). We located the tremor bursts using the slowness vector from the three arrays and a 1-D S wave velocity model (derived from the Pacific Northwest Seismic Network (PNSN) P3 model [Crosson, 1976]) (section 2.3). We analyzed larger time windows (5 min) for the entire duration of the 2004 tremor episode (section 3.1). We then analyzed the short-time scale (30 s) spatial and temporal evolution of tremor locations for a few characteristic time periods (section 3.2). Results from the longer time window analysis are consistent with the shorter window results, thus justifying the computation savings in using longer time windows to complete the analyses for the entire episode. Using the results of our analyses in sections 2 and 3, we discuss source models for tectonic tremor that are consistent with the majority of ours and previous observations (section 4). Our conclusions are outlined in section 5.

2. Data and Processing

2.1. Small Aperture Array Data

[9] From late March through early August 2004, we deployed three seismic arrays to record an anticipated tectonic tremor and slip event: one array was located near Sequim, WA, one on Lopez Island, WA, and one near Sooke, BC (Figure 2). Array locations were chosen to surround the area where the previous repeating Cascadia tectonic tremor and slip events had initiated (Figure 2) [Rogers and Dragert, 2003; McCausland *et al.*, 2005]. The aperture of the arrays (~ 600 m) and inter-station spacings (150–200 m) were chosen based on the strongest frequencies (1.5–4 Hz) and apparent velocities of the tremor (3.8–4.2 km/s) [McCausland *et al.*, 2005].

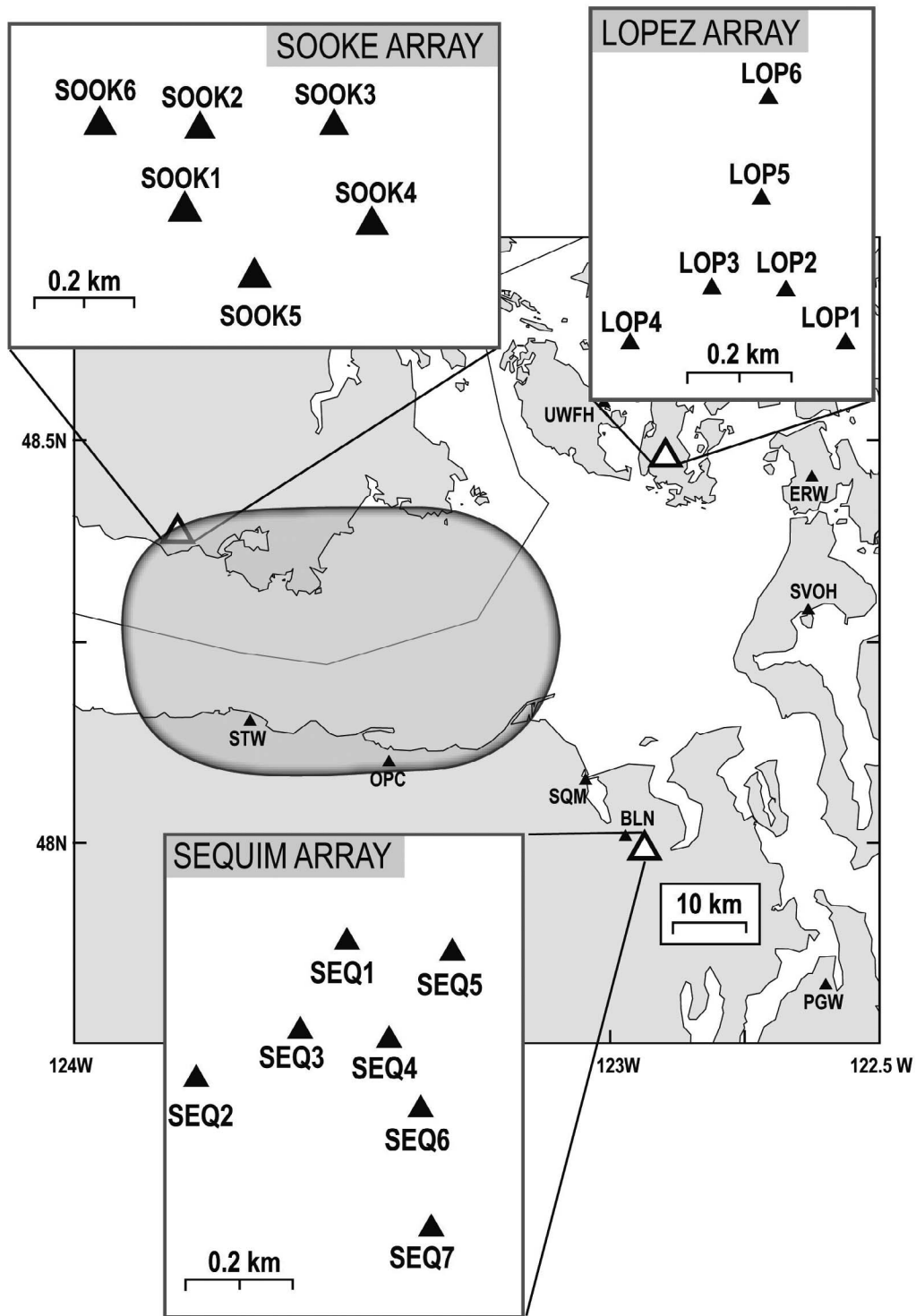


Figure 2. Map showing the location of each array (white triangles), regional network stations (black triangles), and the region where previous tremor and slow slip episodes initiated (gray shaded oval). The inset maps show the station configurations for each array.

[10] The array near Sequim consisted of 7 stations, recorded at 125 Hz: each station using a Lennartz LE-3Dlite 1-Hz seismometer and a Lennartz Marslite data logger. The array near Sooke consisted of six seismic stations recorded at 100 Hz: each station using a 2-Hz L22 seismometer, a

Quanterra Q330 data logger, and a Quanterra baler. The array on Lopez Island consisted of 6 stations recorded at 125 Hz. Lennartz LE-3Dlite 1-Hz seismometers and Lennartz M24 data loggers comprised this array.

2.2. Determination of Relative Arrival Times and the Apparent Slowness

[11] We solved for the apparent slowness using the calculated relative arrival times of the tremor wavefront between station pairs. Each component of each array station was processed separately, and the vertical components were not used because the signal strength was too close to the background noise. Two different window sizes were used to process the data: 5 min and 30 s. The longer window was used to analyze the first 16 days of the sequence, while the shorter window was used to examine finer scale changes in the tremor during shorter, but representative time periods. Details concerning how these window sizes were determined are described in Text S1 in the auxiliary material.¹

2.2.1. Cross-Correlation Analysis

[12] The relative arrival times of the tremor at different stations within each array were determined by cross-correlating the waveforms at all station pairs. Sub-sample time delays were obtained by searching for local maxima in the cross-correlation function, fitting a parabola to the values nearest the maximum, and then calculating the lag time corresponding to the peak of the parabola. Time delays greater than 0.25 s were discarded because they are not realistic for a sub-surface seismic source given the maximum inter-station spacing of 568 m. Each remaining time delay was then used in a weighted least squares linear-regression that solved for the best fit plane wave solution to relative arrival. The weights were determined based on the relative size of the first two cross-correlation maxima.

[13] Following *Aster et al.* [2004], the weighted least squares linear regression can be described using matrices:

$$\mathbf{A}\mathbf{s} = \delta\mathbf{t}, \quad (1)$$

where \mathbf{A} contains the pair-wise station spacing differences in x (east) and y (north) coordinates, $\delta\mathbf{t}$ is a column vector containing the observed lag times between pairs of stations, and \mathbf{s} is a two element vector containing the east and north components of the slowness of an assumed plane wave. Weights are applied to \mathbf{A} and to $\delta\mathbf{t}$ in the following manner:

$$\mathbf{A}_w = \mathbf{C}^{-1/2}\mathbf{A},$$

and

$$\delta\mathbf{t}_w = \mathbf{C}^{-1/2}\delta\mathbf{t}, \quad (2)$$

where $\mathbf{C}^{-1/2}$ is a diagonal matrix whose entries are the reciprocals of the estimated errors in the observed traveltimes differences. We then find the least squares solution of the weighted equation

$$\mathbf{A}_w\mathbf{s} = \delta\mathbf{t}_w. \quad (3)$$

[14] The error in the estimate of slowness can be calculated from the estimated errors in the pair-wise time differences. The covariance of a product between a matrix,

\mathbf{G} , and a vector of random variables, $\delta\mathbf{t}_w$, can be rewritten as

$$\text{Cov}(\mathbf{s}) = \text{Cov}(\mathbf{G}\delta\mathbf{t}_w) = \mathbf{G}\text{Cov}(\delta\mathbf{t}_w)\mathbf{G}^T, \quad (4)$$

where

$$\mathbf{G} = (\mathbf{A}_w^T\mathbf{A}_w)^{-1}\mathbf{A}_w^T, \quad (5)$$

and the weighted data have a covariance equal to the identity matrix. We evaluate the fit assuming the errors follow a normal distribution and are statistically independent, so that the dimensionless weighted misfit,

$$\mathbf{M} = \text{res } \mathbf{C}^{-1} \text{ res}, \quad (6)$$

has a χ^2 distribution with an expected value of $N-2$, where N is the number of pairs of seismograms. The residual, res , can be determined from the difference between the observed relative arrival times and those predicted by the estimated slowness,

$$\text{res} = \delta\mathbf{t}_{\text{observed}} - \delta\mathbf{t}_{\text{modeled}} = \delta\mathbf{t} - \mathbf{A}\mathbf{s}. \quad (7)$$

2.2.2. Determination of the Errors in the Relative Arrival Times

[15] Our estimate of the error in the relative arrival times was determined from the normalized interstation cross-correlation functions. The relative sizes of the two largest local maxima of the cross-correlation are used as a measure of the uncertainty of the relative arrival time for a station pair. If two seismograms are well correlated, then the correlation function has one peak that is much higher than any other. If, on the other hand, the two highest peaks of the have similar amplitudes there is a source of coherent noise that is comparable to the signal rendering the observed time lag highly uncertain (an example of the cross-correlations functions is in Text S1). The ratio, R , between the first and second of the correlation maxima was plotted with respect to the time residual of that station pair, err (Figure 3). We fit this plot with a parametric equation as follows:

$$\text{err} = [250^{-1/8} + 0.3(R - 1)]^{-8}/1000. \quad (8)$$

This empirical equation provided a mapping between the ratio of the two largest peaks in the correlogram and the error in the relative arrival time. The estimated error varies from a maximum of 0.25 s ($R = 1$) to a minimum of 0.005 s ($R = 2.05$). These values were used in the weighted least squares slowness inversion described above (section 2.2.1). Figure 4 shows computed slowness values and their errors for 3 h on 11 July 2004 for the three arrays for both 5 min and 30 s time windows.

2.3. Tremor Location Procedure

[16] The tremor locations were determined by minimizing the misfit between the array-calculated slowness values and those predicted by rays traced through a velocity model from trial locations. We used a 1-D linear-gradient S wave model based on the regional P wave velocity model (P3 model used by the PNSN to locate local and regional

¹Auxiliary materials are available in the HTML. doi:10.1029/2008JB006063.

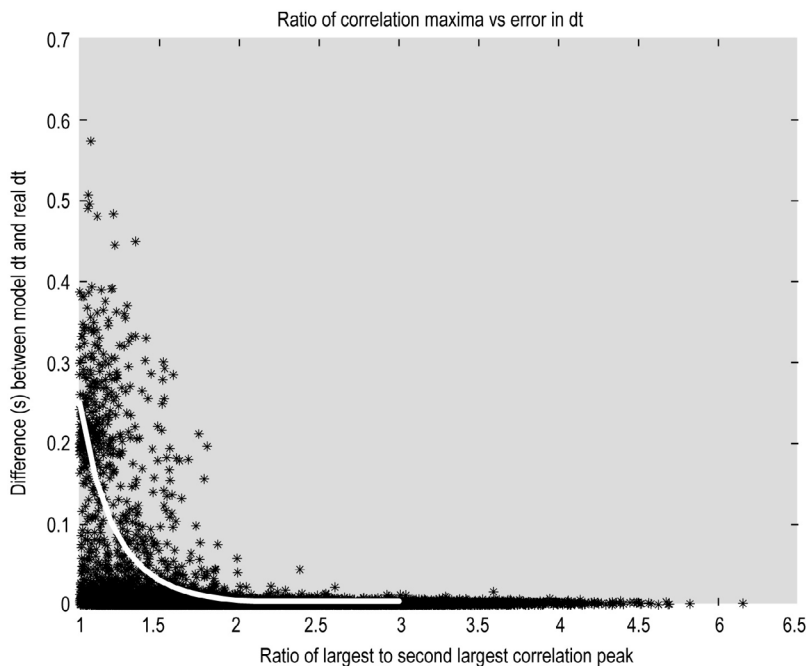


Figure 3. Plot comparing the ratio of the amplitude of the largest two cross-correlation peaks to the absolute value of the relative arrival time residual (difference between the modeled and observed relative arrival times). Data for this plot come from all 5 min time windows on 11 July 2004. The white curve represents the best empirical fit to these data, as cited in equation (8).

earthquakes [Crosson, 1976] and a constant V_p/V_s equal to 1.75 [La Rocca *et al.*, 2008]. An S wave model was used because the majority of energy contributing to tremor recorded on horizontal components is from SH waves [La Rocca *et al.*, 2005].

[17] The traveltimes and slowness vector at each array for the 1-D model were calculated using the Java software

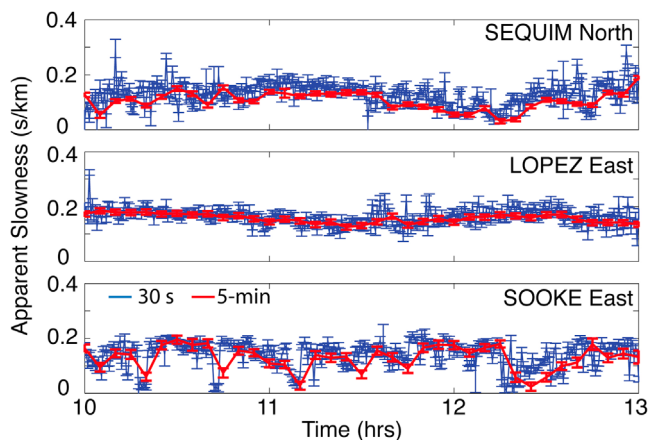


Figure 4. Plot of the array computed slowness and errors that compares the results from the 30 s (blue) and 5 min (red) analysis windows for 3 h on 11 July 2004. Variations in the slowness with time are evident, indicating changes in the location of tremor sources. Despite the large difference in window size, the computed values of the slowness for each are comparable to within the errors, thus demonstrating that the 5 min windows are a reasonable proxy for the 30 s windows.

package TauP [Crotwell *et al.*, 1999]. The S wave velocity model is shown in Table 1. The traveltimes and slowness were computed for a series of depths and a range of distances for the first arriving S wave phase. The calculated values were interpolated to obtain the slowness and traveltimes between points in a regular grid and the centroid of each array. The grid spacing was 5 km in x-y and 3 km in depth. The origin of the grid was 11 km above sea level at 46.25° north and 124.5° west, and the grid extended 245 and 275 km in longitude and latitude, respectively, and to a maximum depth of 88 km below sea level.

[18] The source locations were derived by minimizing the χ^2 misfit (hereafter referred to as misfit) between the observed and calculated slownesses for the three arrays, which for this data set can be represented as follows:

$$\mathbf{M}(\mathbf{x}) = [\mathbf{S}_{\text{obs}} - \mathbf{S}_m(\mathbf{x})]^T \text{Cov}(\mathbf{S}_{\text{obs}})^{-1} [\mathbf{S}_{\text{obs}} - \mathbf{S}_m(\mathbf{x})], \quad (9)$$

Table 1. One-Dimensional Velocity Model^a

| Depth (km) | S Wave Velocity (km/s) |
|------------|------------------------|
| 0.0 | 3.06 |
| 4.0 | 3.17542 |
| 6.0 | 3.6373 |
| 6.5 | 3.68349 |
| 12.5 | 3.80473 |
| 18. | 3.88556 |
| 22.5 | 3.96062 |
| 33 | 4.01258 |
| 39 | 4.09918 |
| 42 | 4.44559 |
| 410 | 4.7 |

^aVelocity model used for 1-D traveltimes and slowness calculations, derived from PNSN P3 model [Crosson, 1976].

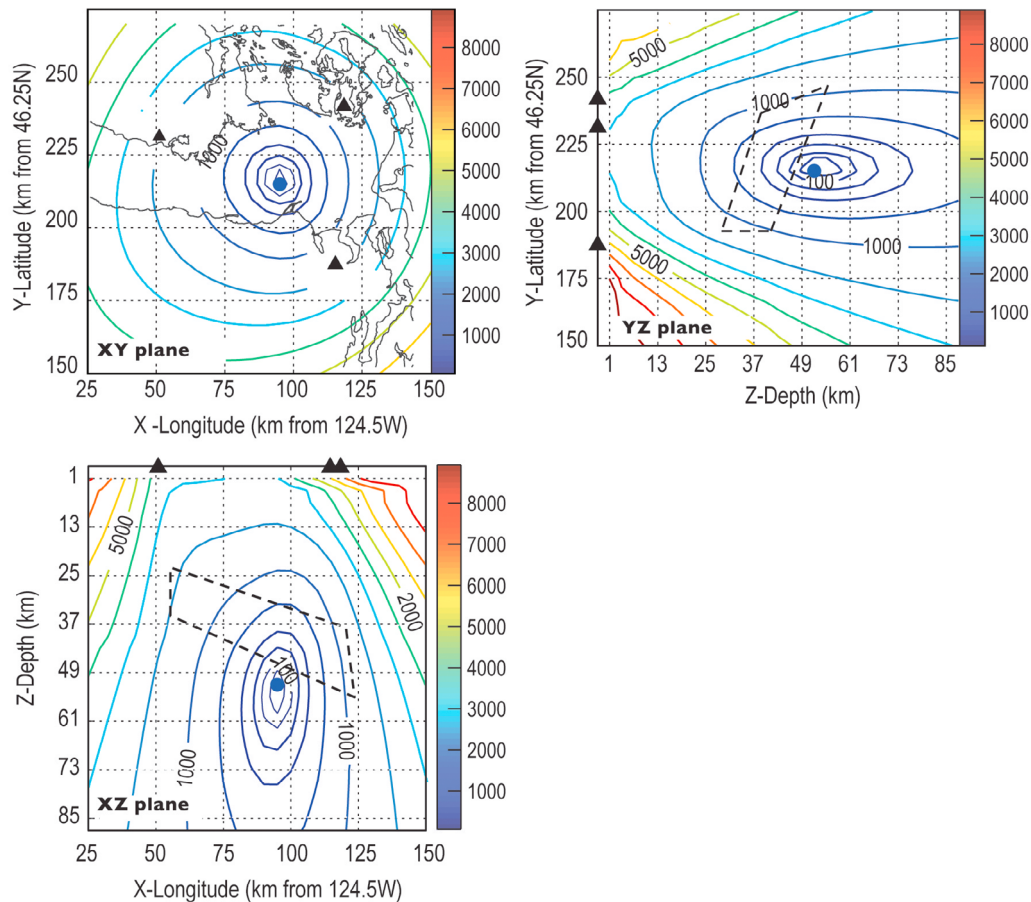


Figure 5. Contours of the misfit between the observed and predicted apparent slowness vectors for one 5 min time window starting at 1525 UTC on 11 July 2004. The contours are shown for the X-Y, X-Z, and Y-Z planes, with the best misfit (location) shown as a blue circle. The locations of the arrays are shown as black triangles, the coastline is plotted for reference on the X-Y plane, and the projection of the subducting slab interface [Preston *et al.*, 2003; Medema, 2006] is indicated by the quadrilaterals on the X-Z and Z-Y planes. The projection represents the slab interface along profiles taken in the south at the latitude of the Sequim array, in the north at the latitude of the Lopez array, on the west at the longitude of Sooke array and on the east at the Lopez array. Between the three arrays, the slab dips roughly to the northeast. Plotted contours are at misfit values of 75, 100, 150, 250, 500, and 1000–9000 in increments of 1000, and the color of the contour signifies its value (see color bar).

where M is the misfit for a given grid point \mathbf{x} and \mathbf{S}_{obs} and \mathbf{S}_m are column vectors containing the 12 observed and model predicted values of the east-west and north-south components of slowness at each of the two horizontal channels on each of the three arrays. Our χ^2 statistic has 10 degrees of freedom with an expected value of 10 and should be 16.0 at least 90% of the time. However, our misfit values are larger (by at least a factor 5–10) than predicted by the χ^2 distribution. This is likely a result of the coarseness of the grid, underestimating the uncertainties in slowness, not considering errors in the wave speeds (which in truth is 3-D), and, time windows in which the slowness calculated on the east and north components differ by more than the estimated error.

[19] Thus we took a Bayesian approach to understanding the error in our locations [Aster *et al.*, 2004]. We rescaled the probabilities of obtaining all the locations within the grid such that they added up to one. We summed the probabilities in ever-expanding concentric ellipsoids to determine the area

of 90% confidence. The major axes of the ellipsoids are used to estimate the uncertainty in the location (Figure 5). The average of the errors in the best locations (misfit < 100) between 6 and 22 July are of the order of 5–6 km in epicenter and 10 km in depth for 5 min time windows (Table 3). Errors in the locations more generally (misfit < 600) for 5 min time windows are on the order of 13 km in epicenter and 16 km in depth.

3. Tremor Locations and Spatiotemporal Behavior

[20] Observations using network [McCausland *et al.*, 2005] and array processing of the locations and the gross migration of the tremor over many hours to days are consistent. The first tremor bursts in the July 2004 episode located beneath the region of the Strait of Juan de Fuca east of Lopez and Sequim arrays, and subsequent epicenters migrated first in the east and west directions between the

Table 2. Percentage Tremor Occurrence^a

| | Sooke | Sequim | Lopez |
|---|-------|--------|-------|
| 6–22 July 2004, 5 min windows, north | 84.6 | 63.1 | 95.1 |
| 6–22 July 2004, 5 min windows, east | 80.3 | 77.1 | 98.5 |
| 11 July 2004, 0000–0600 UTC, 30 s windows, north | 98.7 | 89.4 | 99.2 |
| 11 July 2004, 0000–0600 UTC, 30 s windows, east | 99.7 | 91.4 | 99.0 |
| 11 July 2004, 2000–2400 UTC, 30 s windows, north | 99.0 | 96.0 | 99.4 |
| 11 July 2004, 2000–2400 UTC, 30 s windows, east | 99.2 | 99.6 | 97.5 |

^aPercentage of 5 min and 30 s time windows in which tremor was detected. Each component and array was considered separately.

arrays at average speeds between 5 and 10 km/d. Then the epicenters migrated bidirectionally along strike, to the south of the Strait under the northern Olympic Peninsula and to the northwest of the Strait under Vancouver Island. This second (bidirectional) migration is the same as was observed from the location of tremor bursts using the PNSN stations [McCausland *et al.*, 2005] and occurred at average speeds of 15 km/d.

[21] Dense seismic arrays are more sensitive to low levels of tremor than the regional network data. From PNSN data, we initially determined that the July 2004 tremor episode in Cascadia began on 8 July and lasted until 24 July in the region of the arrays. However, through the cross correlation of the array data, we determined that the tremor sequence in the region between the three arrays started on 6 July 2004, but by 24 July it had migrated out of the region between the three arrays but could be still detected on the Sooke array through 27 July, when the arrays were dismantled. The large-scale migration of the tremor source occurred at an average speeds between 5 and 15 km/d, similar to results of previous studies [Kao *et al.*, 2006]. The small-scale migration of the tremor source occurred at speeds between 1 and 2 km/min consistent with results in Japan [Shelly *et al.*, 2007]. Cross-correlating the array data in 5 min analysis windows, we observed that tremor occurred during most hours (at the most, 99%) of the tremor episode (Table 2; locations summarized by day in Text S2). Thus tremor catalogs based on network data alone [e.g., Rogers and Dragert, 2003; McCausland *et al.*, 2005] underestimate the total number of hours of tremor.

[22] The depth distribution of the tremor locations including the errors is wider than would be expected if all of the tremor located on the subducting slab interface [Preston *et al.*, 2003; Medema, 2006]. They generally locate relative to the slab interface, but not directly on the interface, similar to previous studies in Cascadia [e.g., Kao *et al.*, 2005, 2006; McCausland *et al.*, 2005]. Rather than attempting to reduce the depth error by using a priori assumptions (e.g., that the tremor sources occur on the plate interface), we have tried to locate events without bias and to rigorously quantify the errors in the depths for the methods used in this experiment.

3.1. Consistency of Results

[23] We used 5 min nonoverlapping time windows to examine the changes in the tremor locations during the entire time period of interest (6–22 July 2004), when tremor was located between the three arrays. We used 30 s time windows

with 18 s overlap for representative time periods to examine the shorter scale changes in the tremor locations and characteristics. Comparing the results from the two analyses reveals that the general characteristics, locations, and errors remain consistent between the 30 s and 5 min time windows (Figure 4). Thus the larger time windows are a reasonable proxy for the 30 s time windows, allowing for a faster and more efficient way to summarize changes over the whole tremor episode. This also suggests that the location of the strongest tremor sources are stationary within the location error (5–16 km depending on misfit criteria, see Table 3) over 5 min, and from day-long plots of the slowness at the three arrays (one example from Lopez array in Figure 6a) the locations are in fact stationary within the errors over minutes to hours. Comparing the errors for the best locations (Table 3) to errors in array-determined earthquake locations in the same region from LaRocca *et al.* [2008] (<5 km in *x* and *y*, < 10 km in *z*), we find that the errors agree reasonably well.

3.2. Spatiotemporal Evolution of the Tremor, 6–22 July 2004

[24] The tremor began beneath the Strait of Juan de Fuca on 6 July and persisted there through 11 July 2004. During these first days, the majority of tremor epicenters were confined to within a small region (~250 km² on any given day), where on a day-to-day scale, the tremor epicenters migrated between a region east of Lopez and Sequim and a region to the west between the three arrays separated by a distance of about 50 km (see Text S1). Average speeds of these migrations are between 5 and 10 km/d. The depths of the tremor range primarily between 40 and 60 km on 8 July through 11 July. Depths are generally, but not always, deeper to the east during these days suggesting that the tremor locations maintain, at the very least, a similar relationship to the plate interface. The shallowest depths are on 6 and 7 July, the beginning of the episode.

[25] On July 11 the epicenters are in the same region as the previous days (Figure 7), but the signal amplitudes are stronger and we obtained more locations. By 12 July, the epicenters cover a larger region 50 km in latitude from Sooke to Sequim (e.g., see Figure 8 and Text S2). At this point, despite the fact that the amplitude of the tremor is at its largest, the locations of the tremor have larger errors, particularly in depth with many of the events locating at the bottom edge of our grid. Such depths are not considered reasonable. In the 5 min window results, the tremor moved around within this region smoothly on an hourly time scale, but without any specific pattern (such as upwards or downward, along a line or outward from a given point). This

Table 3. Location Uncertainties^a

| Misfit | X Error (km) | Y Error (km) | Z Error (km) | N |
|--------|--------------|--------------|--------------|------|
| <100 | 5.0 ± 3.4 | 6.4 ± 3.4 | 10.1 ± 4.6 | 62 |
| <200 | 7.7 ± 3.8 | 7.6 ± 3.7 | 11.8 ± 5.0 | 342 |
| <400 | 10.9 ± 5.2 | 10.2 ± 5.1 | 14.5 ± 5.4 | 1160 |
| <600 | 13.1 ± 6.5 | 12.1 ± 6.4 | 15.7 ± 5.7 | 1811 |

^aUncertainty in the locations for 5 min time windows for different misfit values. The number, N, of events used in the calculation (locations that meet the misfit criterion) is indicated.

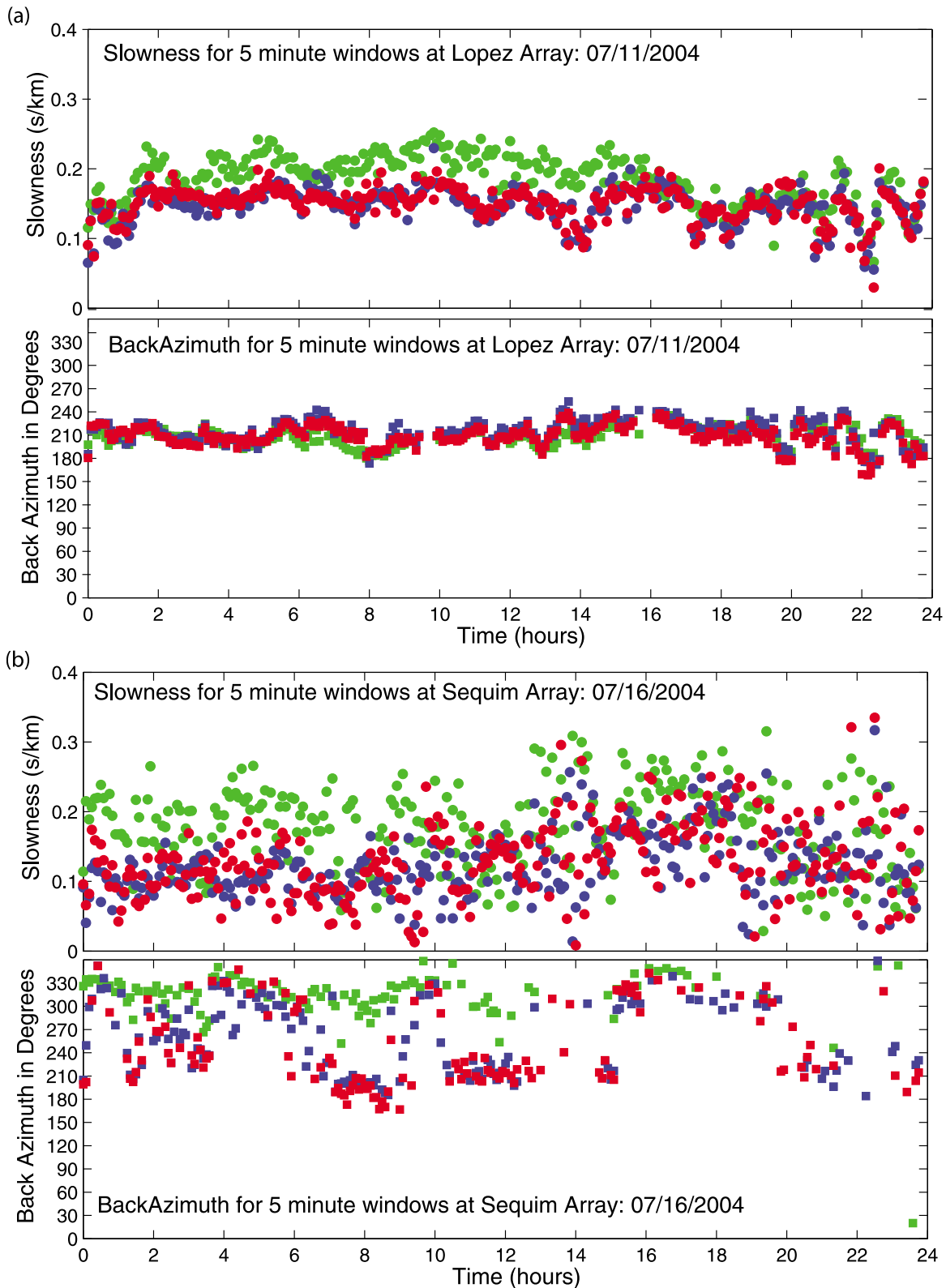


Figure 6. (a) A time series plot of the slowness and back azimuth calculated in 5 min windows at Lopez array on 11 July 2004. Colors represent the slowness calculated for each sensor component: red is north; blue is east; green is vertical. For most of the day the calculated slowness and back azimuths vary slowly over ranges of around 0.1 s/km in slowness and 60° in back azimuth, indicating a single but slowly changing source region for the tremor sources. (b) The time series for 5 min time windows at Sequim array on 16 July 2004. Plot shows sharp changes ($\sim 120^\circ$) in the back azimuth indicating the presence of multiple active source regions, particularly during the first 12 h of the day.

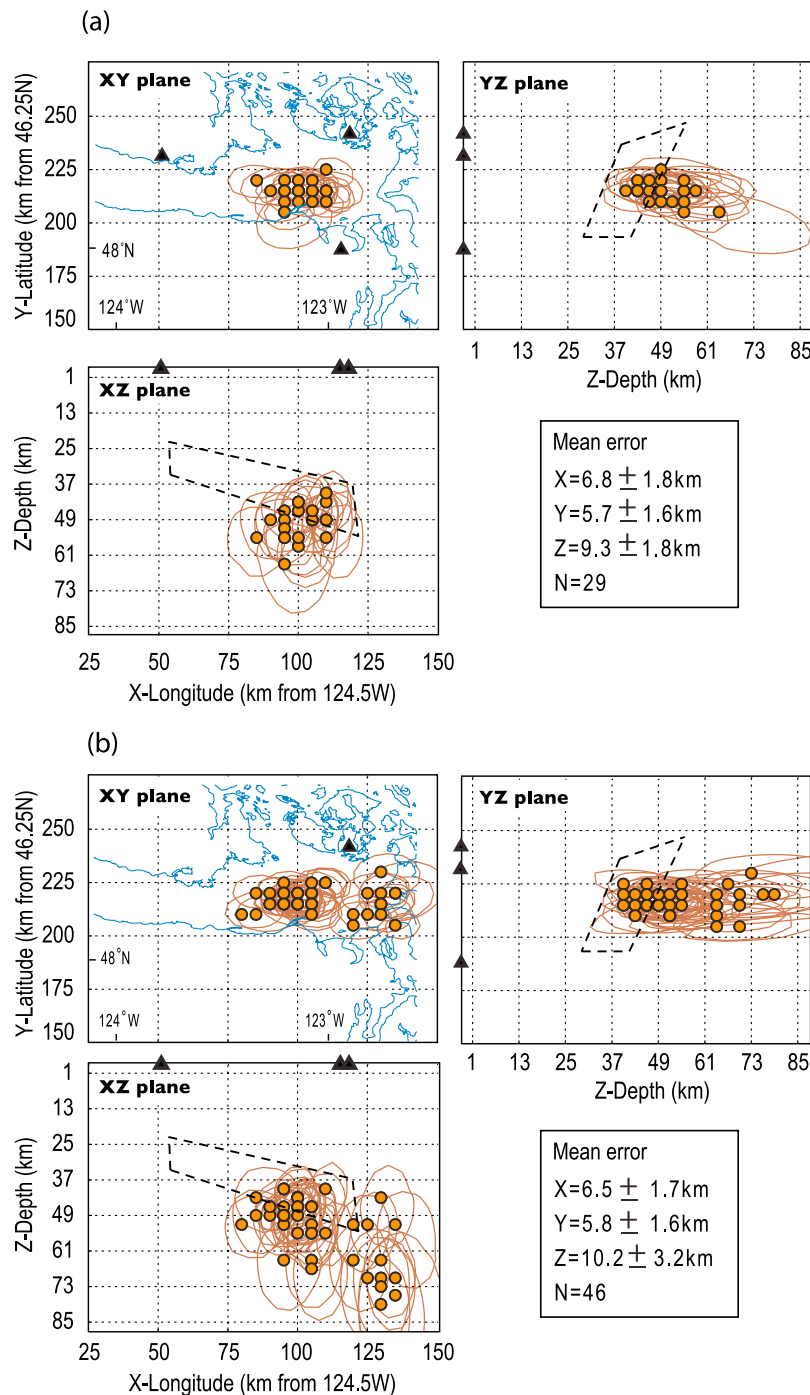


Figure 7. (a) The 5 min time window locations with misfit <200 from the first 12 h of the day on 11 July 2004. (b) The locations from the second 12 h of the day. The location error as defined by the 90% confidence interval is plotted as an ellipse around the location. Mean errors are indicated as is the number of events, N . Two distinct clusters of locations are present in the second 12 h. The coastline is plotted for reference on the X-Y plane, and the projection of the subducting slab interface [Preston *et al.*, 2003; Medema, 2006] is indicated by the quadrilaterals on the X-Z and Z-Y planes. The quadrilateral is on the plate interface with vertices at the three arrays and at the point defined by the latitude of the Sequim array and the longitude of Sooke array.

time period shows more complicated migration pattern in the 30 s time windows discussed in section 3.3.

[26] The apparent widening of the tremor region on 12 July coincided with the time periods in which multiple sources

began to be evident from network locations [McCausland *et al.*, 2005] and from beam-forming analysis at the arrays (the tremor data are stacked at all possible apparent slownesses) (Figure 9). Beam-forming analysis from 15 July

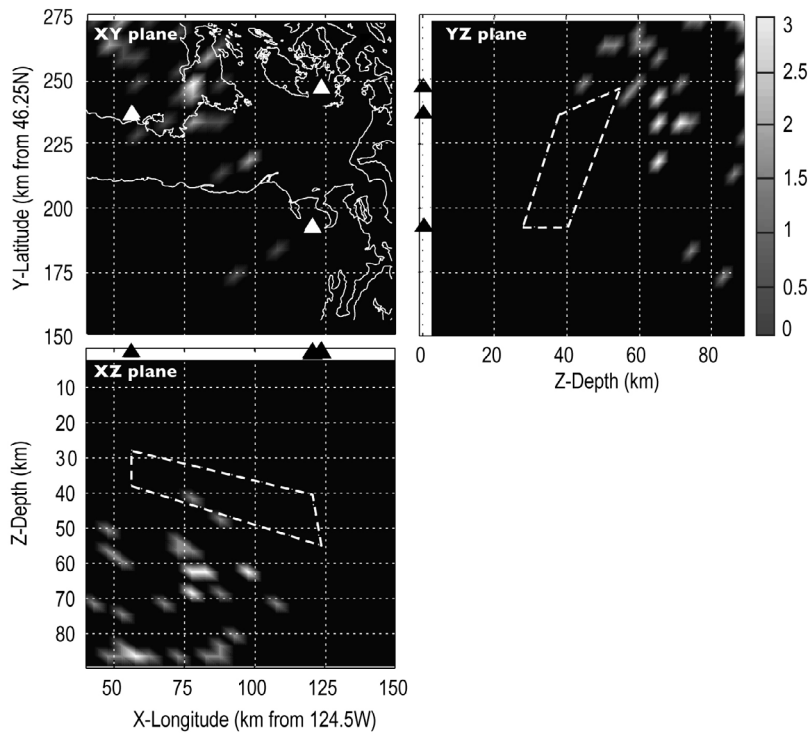


Figure 8. Five-minute time window locations from 15 July 2004, with misfits < 300 plotted as 2-D histograms projected onto X-Y, X-Z, and Y-Z planes. The number of locations at any particular grid point is indicated by the gray scale value as indicated on the color bar. The coastline and slab projections are indicated as described in Figure 5. Epicentral locations are more geographically distributed and generally closer to the Sooke array. Depths are deeper and less well constrained than for previous days.

shows that at the Sequim array there were tremor sources to the northwest and southwest (Figure 9). At Sooke array, the sources were to the northeast and southeast of the array. For both arrays, these back-azimuth directions are consistent with array-determined source locations (Figure 8). Multiple sources were most common between 12 and 17 July, and are easily observed on the Sequim and Sooke arrays. Multiple source regions complicate our ability to locate the tremor with the method because our analysis picks out the strongest source in any given window at each array. The strongest sources might be different at each array, therefore the method may not be able to resolve a location that satisfies the calculated slowness at all three arrays. This greater distribution of locations during these days made the hourly scale temporal progression harder to follow: the source that is the strongest in one window may not be the strongest in the next window (Figure 6b). This will cause the temporal progression from window to window to appear more chaotic or sporadic than it truly might be.

[27] Between 17 and 24 July, the tremor located primarily around and to the northwest of the Sooke array. Depths during this time period were poorly to completely unconstrained because the Lopez and Sequim arrays were too far away from the tremor source to help constrain the depth. The epicenters had migrated out of the area of robust constraints (between the three arrays) by 24 July, but tremor could still be detected through 27 July when the last array, Sooke, was dismantled.

[28] Figure 10a shows all locations with a misfit less than 200 for the time period between 6 and 22 July; average

errors in these locations are 8 km in the east-west and north-south directions and 12 km in depth. For comparison all locations with no misfit cutoff are plotted on Figure 10b. The locations are all within the same region and depths, including events with large errors (> 20 km). Text S2 includes two-dimensional histograms of the locations for 6 to 22 July for 5 min time windows. The location errors in the supplement averaged over all days are < 11 km in x and y directions, < 15 km in depth. The errors in the locations were determined for the 5 min time windows from the size of the 90% region of the Bayesian modified misfit calculation.

3.3. Spatiotemporal Evolution of Tremor on 11 and 15 July 2004

[29] To examine the spatial and temporal progression of the tremor on a time scale on the order of minutes, we looked in greater detail at windows in the early days of the sequence when the tremor was located between the three arrays and seemed to be isolated to a small region (see Text S2). We used 30 s long windows with an 18 s overlap; the overlapping 30 s time windows ensured that the same tremor source was included within the time window at each array, for sources located between the three arrays. There was just one source active in a given time window during the first days of the tremor episode (6–11 July 2004), and the direction and slowness of the waves from a source were steady over time periods of 20–30 min or longer (Figure 6a). Changes in the direction and slowness (which relate to changes in location) occurred gradually and systematically over time periods of 2 to 4 h; they did not occur abruptly or

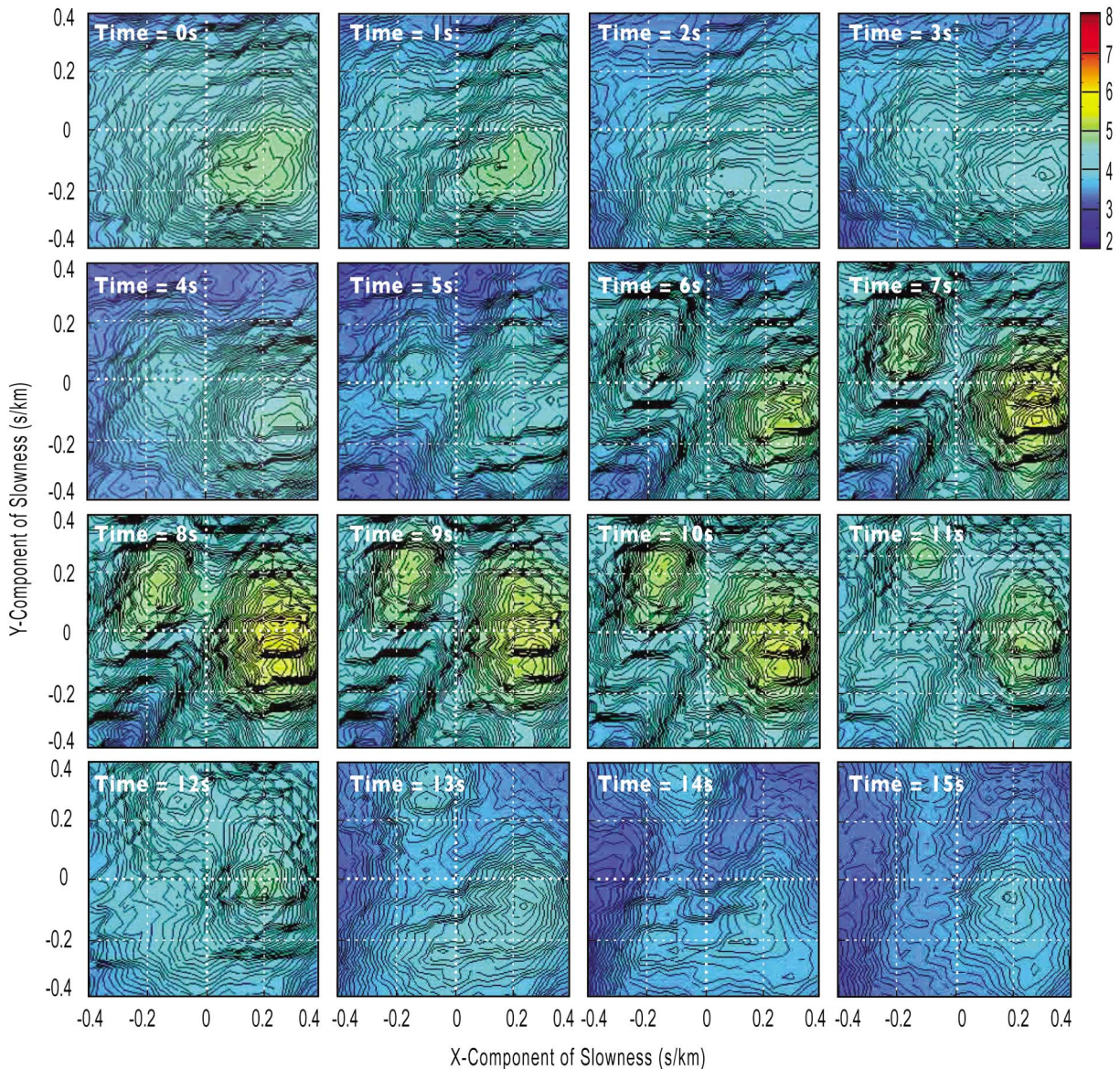


Figure 9. Time series view of beam-forming results in the apparent slowness plane for the east components of Sequim on 15 July 2004. The analysis time window is 5 s, and the time between windows is 1 s (i.e., a 4 s overlap). Color indicates the relative power of the stack at each value of apparent slowness (reciprocal of velocity), where warmer colors indicate coherent energy arriving at the array from a particular direction with a particular apparent speed. For instance, if a wave were vertically incident, then the apparent slowness would be zero and the corresponding peak would plot in the center of the above images. At least two strong tremor sources are clearly evident in many of the time windows. Between 4 s and 8 s, the left tremor source migrates in the slowness plane from 0 to 0.2 s/km in the y direction indicating a change in location. Changes in slowness also occur within 1 s; for instance, between 12 s and 13 s the apparent slowness of the right source changes from approximately 0 to -0.1 s/km in the y direction.

chaotically. Changes in azimuth that did occur were within $30\text{--}60^\circ$; changes in slowness were within 0.15 s/km.

[30] On 11 July 2004, tremor amplitudes were the largest for the times when the source region was spatially limited (Figure 7). We examined the first 5 h of 11 July in 30 s time windows with an 18 s overlap (Figure 11). Results are consistent with those obtained from the non-overlapping 5 min windows (Figure 7). The locations moved around within roughly 15 km in latitude, 40 km in longitude and 20 km in depth. From one time window to the next, the

locations do not change greatly: the average change in the epicentral location was 7 ± 6 km, and the average change in depth was 5 ± 5 km. This made determining an average migration speed difficult, but at most the sources moved 10 km/h. Only in the later days of the episode (after 12 July), when the tremor migrates bi-directionally, do the shorter analysis windows show more extreme variations in the location of the tremor source.

[31] During the last hours on 11 July 2004, there was more than one active source region (Figure 7), therefore we used

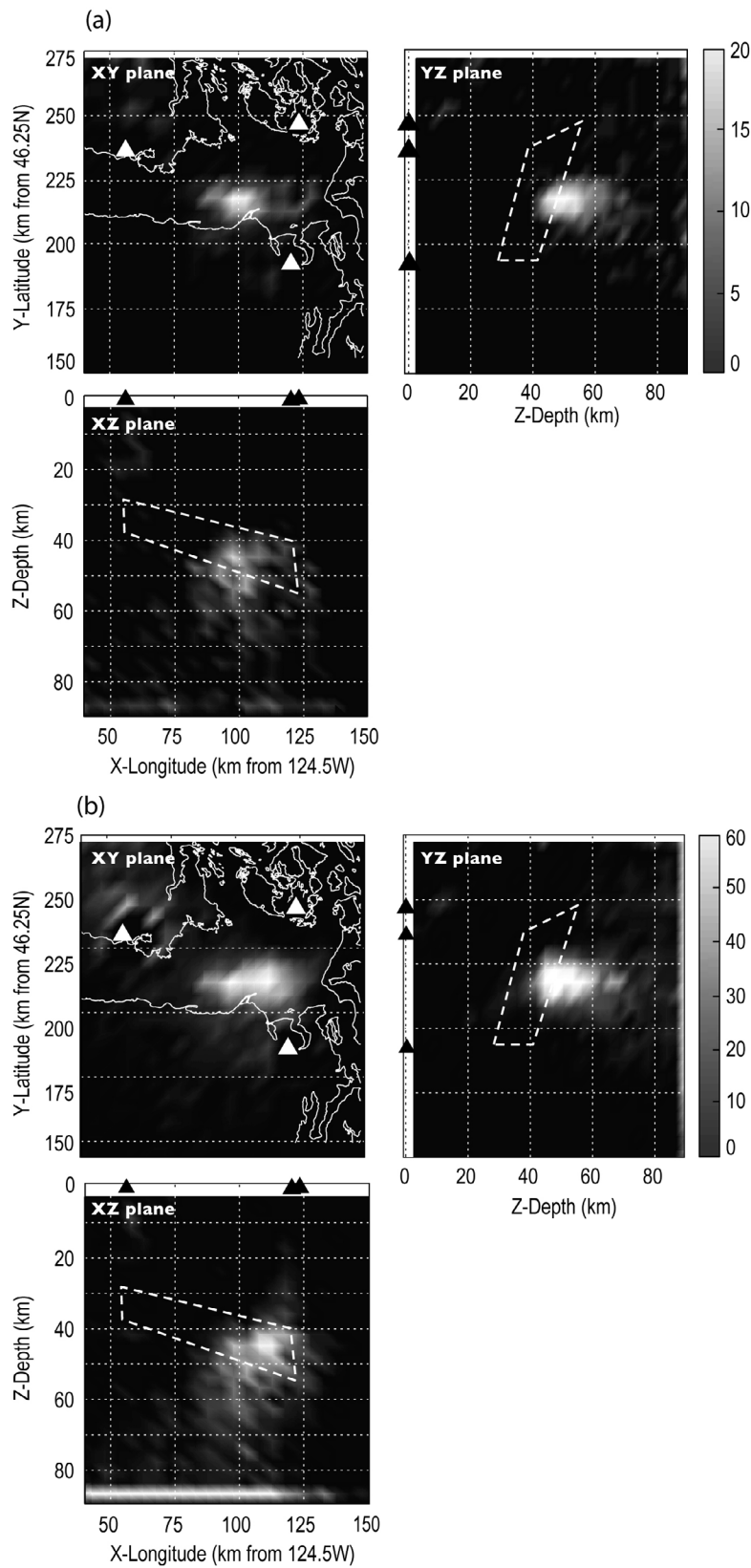


Figure 10. Spatial 2-D histogram of all locations from 5 min time windows between 6 and 22 July 2004. (a) A strict misfit cut off (< 200) for plotting the location. (b) No cutoff for plotting the location and therefore shows more locations but with larger errors. Despite the difference in the errors, the locations are consistent between Figures 10a and 10b. The coastline and slab interface projections are indicated as described in Figure 5.

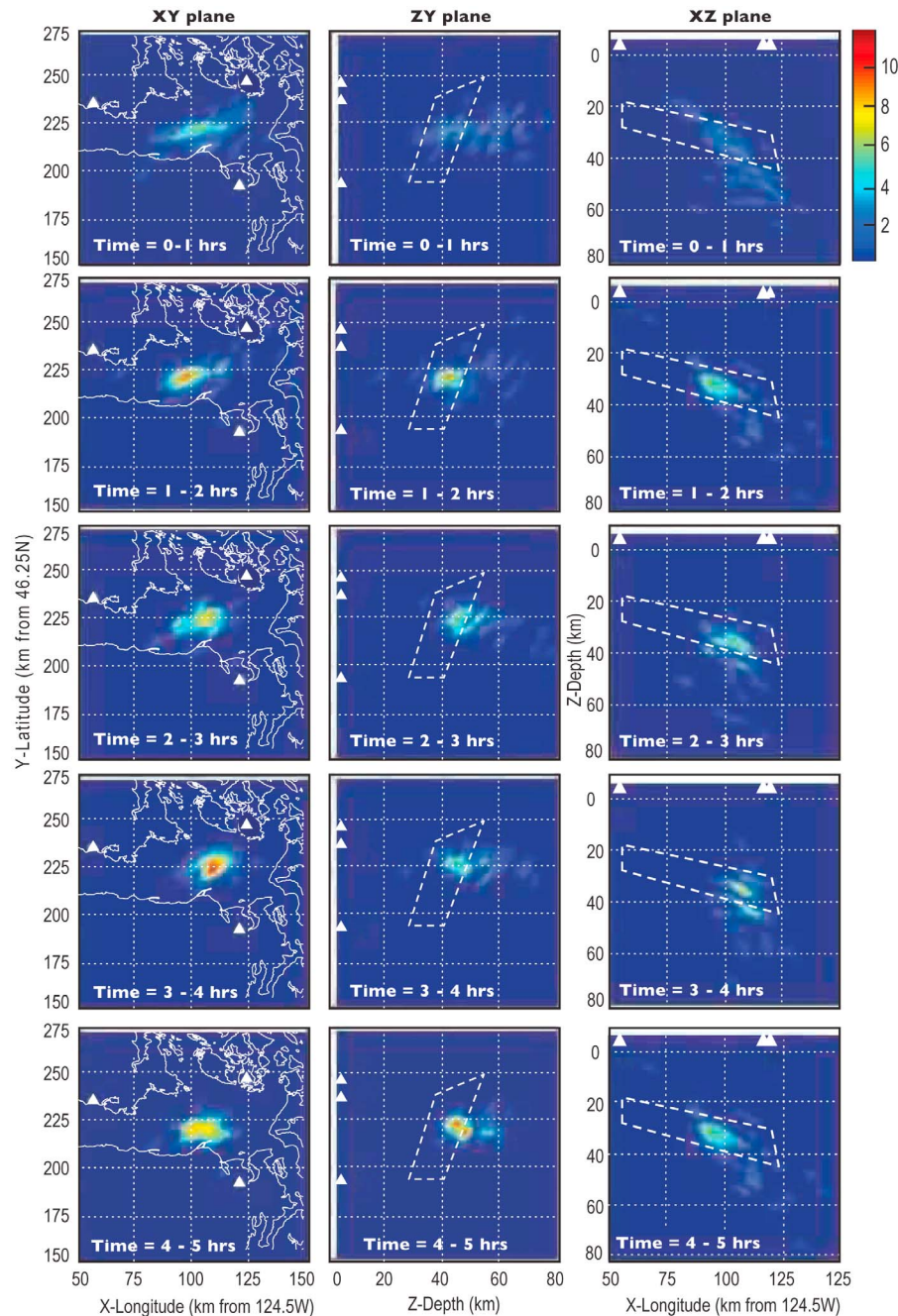


Figure 11. Filmstrip representation of changes in tremor locations during the first 5 h on 11 July 2004. Each column is a 2-D histogram of locations in one of the three coordinate planes, with the number of sources at each grid point indicated by the color as indicated in the color bar. Each plot represents 1 h of locations determined in 30 s windows with 18 s overlap. From hour to hour, the concentration of tremor sources moves around within an area 15 km in latitude, up to 40 km in longitude, and 20 km in depth.

30 s time windows with a 10 s overlap to investigate the epicenter transition between these two regions or whether the two regions were simultaneously active. Figure 12 shows a filmstrip representation of consecutive 5 min summaries of locations for 30 s analysis windows. The transition of the tremor from one region to another occurs between 2100 and 2200 UTC. The tremor does not simply jump from one region to another, but the movement is not smooth either. The epicenters move generally west to east, back west, and

then stay to the east for a few hours. The initial three and final two frames show the migration is not perpendicular to strike (roughly northeast), rather it is in the east-west directions. The majority of the intervening frames show movement in the up- and down-dip directions. The speeds of these migrations range from 1 to 2 km/min, regardless of direction. Source depths are deeper than the slab, but are deeper in the down-dip direction, consistent with the shape of the slab.

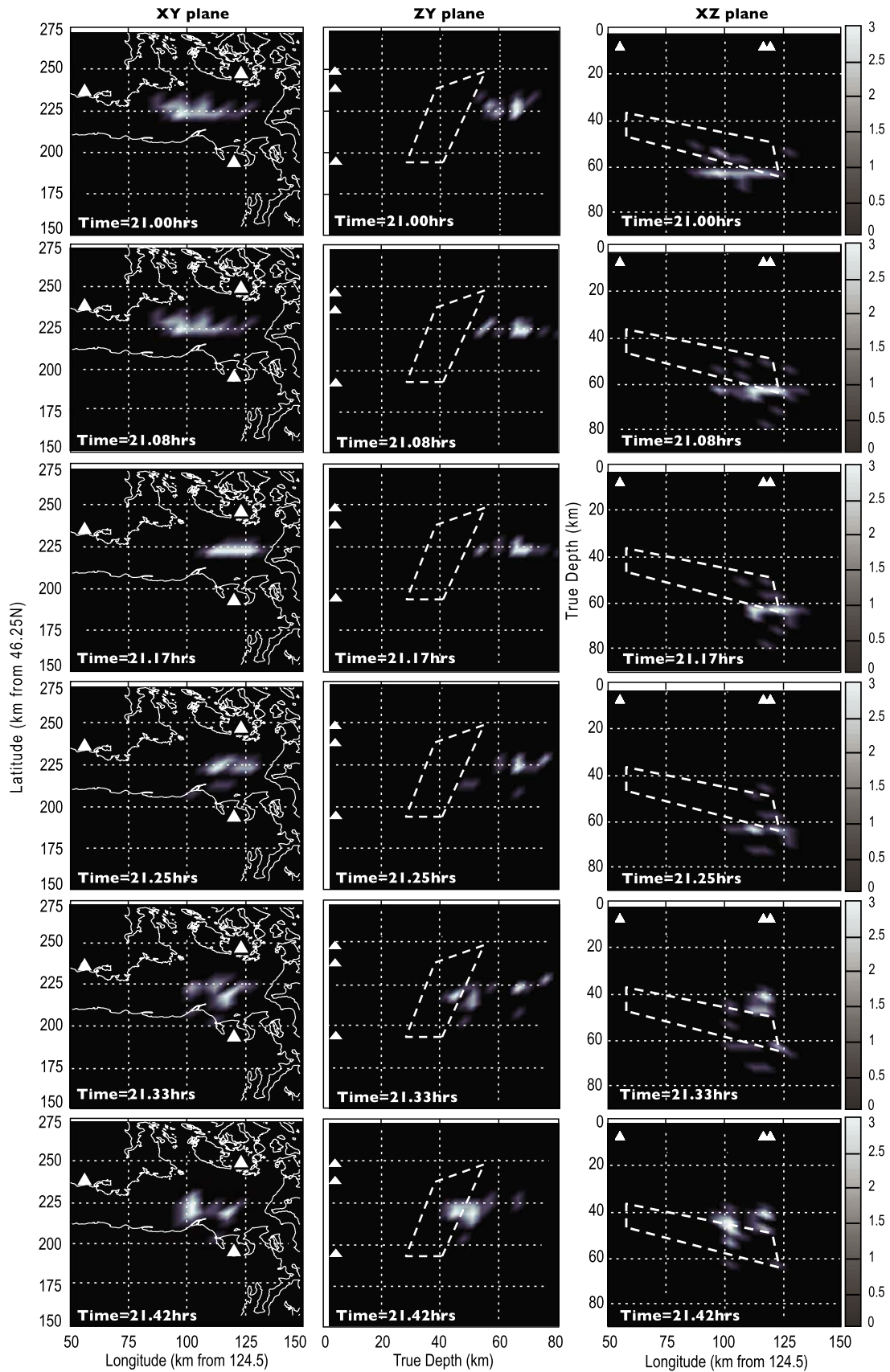


Figure 12

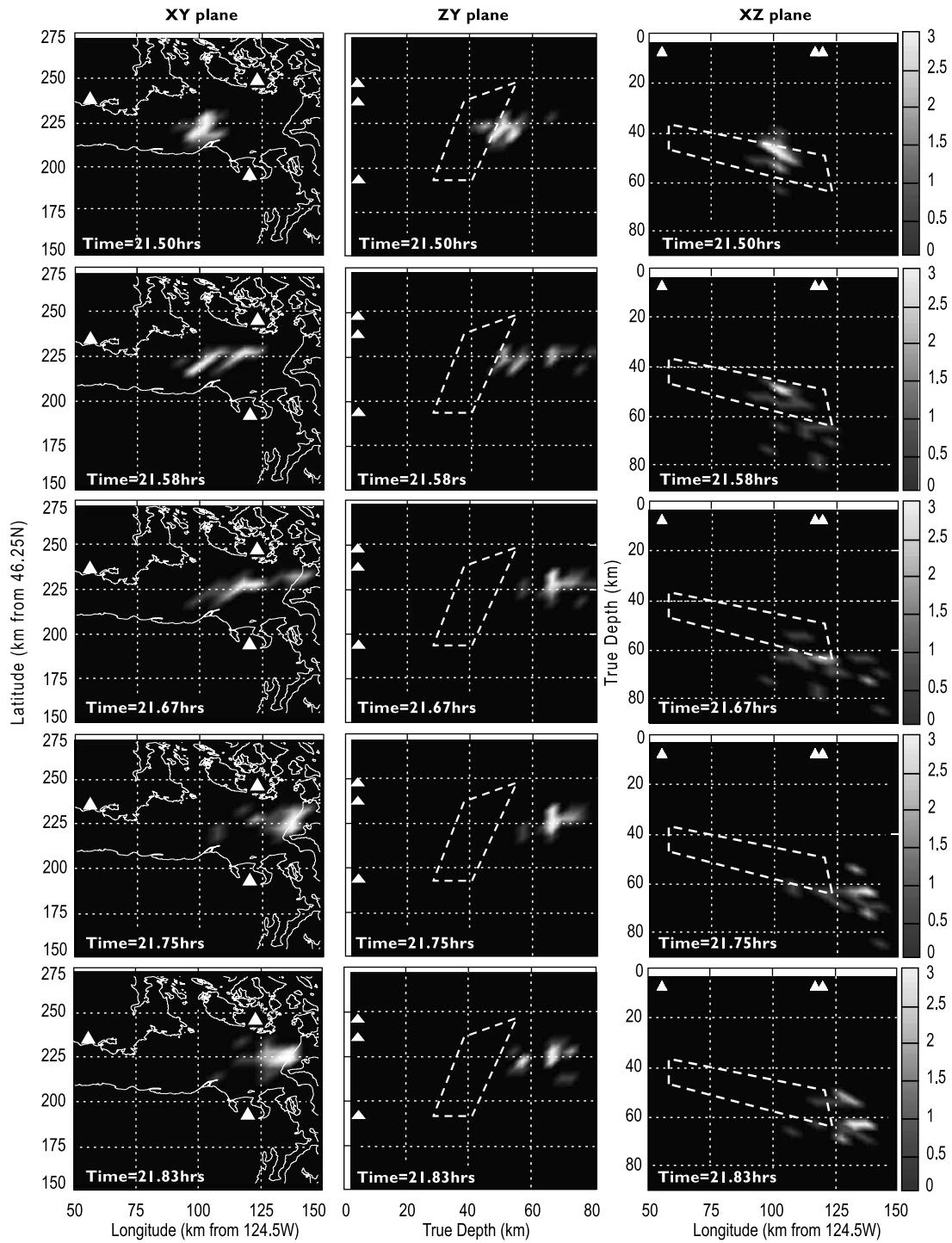


Figure 12. (continued)

Figure 12. Filmstrip 2-D histogram representation of 30 s locations (misfit < 300) in successive 5 min windows between 2100 and 2200 (UTC) on 11 July 2004. (left) The locations in the X-Y plane, (middle) the Z-Y plane, and (right) the X-Z plane. Each frame represents all locations within a 5 min period, the value of the shading indicates the number of sources at a given grid point as indicated by the color bar. How the tremor locations migrate from one source region (between the three arrays) to another source region (east of Lopez and Sequim arrays) is shown. Coastline and slab projections are shown as described in Figure 5.

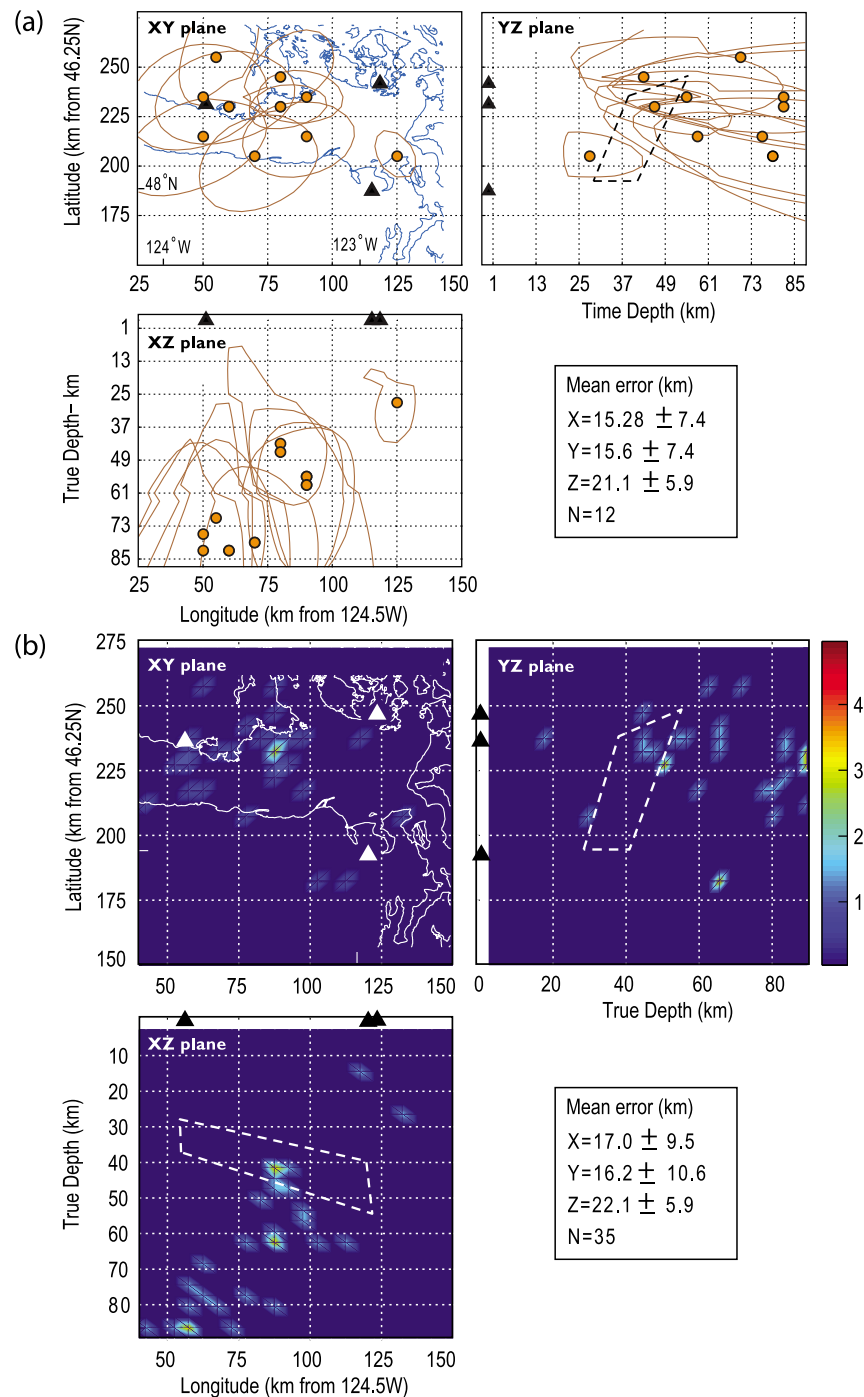


Figure 13. Figure of 30 s locations during a time period with multiple coincident source locations on 15 July 2004. (a) Location and confidence interval for misfits <100 between 0800 and 0900 UTC on 15 July 2004. (b) A 2-D spatial histogram of locations for the same time period, but for misfits <600, with the number of sources at any grid point indicated by the color. Average errors in the locations for each case are indicated. Note that the location errors are larger and the epicentral locations are closer to the Sooke array and distributed over a larger region than on previous days. Coastline and slab interface projections are as described in Figure 5.

[32] Finally, we examined a day in which there were several different tremor sources active at any given time knowing we would be able to resolve fewer locations even though the tremor amplitudes were at their largest. When the tremor data are stacked at individual arrays for all pos-

sible apparent slownesses (beam-forming), multiple source regions are clearly resolved (Figure 9), a result which is consistent with network-determined locations [McCausland *et al.*, 2005] and consistent with times when the first two peaks of the cross-correlation function are of similar mag-

nitude. Locations from just 1 h on 15 July for 30 s time windows are shown in Figure 13. Figure 13a shows the best locations (misfits < 100) with their 90% confidence region. The location errors are larger than for the same misfit criterion on 11 July, and with the exception of one location, the depth error is essentially unconstrained. Figure 13b shows a histogram of more locations (misfits < 600), which gives a better indication of the source distribution. The sources cover a much larger region than in earlier days of the tremor episode: near Sequim there are three sources, one to the northeast of the array and two to the southwest; near Lopez there is one to the southwest; while near Sooke the sources cover a 180° arc clockwise between the northeast and southwest directions.

4. Interpretation and Discussion

[33] The goals of our experiment were to better locate the tremor, to track the progression of tremor sources during an ETS event, and thus to better understand the source of the tremor and how it relates to the processes at plate boundaries. In this section, we will comment on the results from this small-aperture seismic array experiment, and evaluate two working hypotheses for the tremor source, taking into account the tremor observations, GPS observations and other geochemical and geophysical observations found in Cascadia and other warm, young subduction zones.

4.1. Comments on Results From This Experiment and Previous Network Observations

[34] From the array data we observe that the migration of tremor hypocenters on a several day time scale is not smooth, but rather the hypocenters are localized to within 15 km horizontally and 20–40 km in depth for several days, and then the active volume rapidly (within hours) shifts to a new position. Our detailed analysis allowed a raw estimate of the migration velocity, which in some cases yields values up to 2 km/min. This value reveals a small scale behavior of the tremor quite different compared with the much slower migration estimated at regional scale. The depths observed with the arrays in this experiment (30–70 km) are slightly deeper than the network depths (12–60 km) [McCausland *et al.*, 2005; Kao *et al.*, 2006]. While the array locations do not fall precisely along the modeled subducting slab interface, they do seem to better mirror the slab interface than the network locations.

[35] The lack of shallow (12–30 km) array-determined locations could be an artifact of using only direct S wave phases to calculate the model slowness values. In other words, only the first arriving upgoing (s) or downgoing (S) direct S wave was used to calculate the theoretical slowness vector for each grid point to each array—no converted phases were considered (e.g., sS, pS, etc). However, this assumption may cause deeper depths to be assigned to those shallow sources whose first arriving phases are converted phases, such as tremor sources whose distance from the array is great compared to the depth. Therefore this assumption will preclude shallower sources.

[36] Location solutions for the 1-D velocity model have the smallest errors when there is a single tremor source region active at one time, and location solutions become almost impossible to determine with the present methodology when

multiple source regions are active. The presence of multiple active source regions can be seen in the network data, in the 5 min cross-correlated time windows [McCausland, 2006], and from beam-forming analysis on 5 s overlapping time windows where the source location can change over 1 s (Figure 9). Therefore a more sophisticated methodology needs to be developed to track the tremor when it resolves into simultaneous multiple source regions near the arrays.

[37] The same signal characteristics are observed as from network data, and some network-scale observations are important to our discussion of possible tremor source models. Average reduced displacements [McCausland *et al.*, 2005] for tremor with and without a known slow slip event are similar indicating that the amplitude of the seismic signal is independent of whether a detectable slip event occurs. However, the epicentral regions for the Cascadia tremor events without slip are smaller than those with slip, suggesting that if the tremor and slip always occur together then perhaps the slip patch is below the current resolution of regional GPS networks. On the time scale of days and over great distances (hundreds of kilometers), the network-determined tremor epicenters are consistent with the progression of previously modeled slow slip events [e.g., Dragert *et al.*, 2001; McCausland *et al.*, 2005; Kao *et al.*, 2007]. However, on shorter time scales (minutes to hours), the source locations are more chaotic (this experiment and McCausland *et al.* [2005] and Kao *et al.* [2006]). Finally the tremor can migrate bi-directionally from the point of initiation.

4.2. Comments on Other Seismic, Geophysical, Geodetic, Geochemical Data Relevant to the Mechanism of Tectonic Tremor in Cascadia

[38] A comprehensive physical model of tectonic tremor must account for a number of constraints from the seismic signals themselves and from our analysis of the spatial and temporal properties of the tremor. In this section we start our discussion of models with a brief summary of the constraints we have developed and of those from previous geophysical, geodetic, seismic and geochemical studies. The general seismic character of tremor can be summarized as low band-limited frequency content, emergent-onset, long-durations, small-amplitudes, dominance of the waveform by S waves [e.g., Obara, 2002; McCausland *et al.*, 2005; Kao *et al.*, 2006], and embedded low frequency earthquakes within the tectonic tremor signal [Shelly *et al.*, 2006; La Rocca *et al.*, 2009]. The spatial and temporal characteristics of Cascadia tectonic tremor are frequent concurrence with cyclic geodetically measured slow slip events [Rogers and Dragert, 2003], overall migration of tremor epicenters on several day times scales [Rogers and Dragert, 2003; McCausland *et al.*, 2005; Kao *et al.*, 2007], depth distribution of locations greater than the depth variation of the subducting slab (McCausland *et al.* [2005], Kao *et al.* [2006], and this experiment), persistence of tremor within a localized volume on the time scale of hours, presence of multiple active source regions in very short (2 s), short (30 s), and long time windows (5 min), and independence of size (average reduced displacements) for a given episode from measured geodetic slip [McCausland *et al.*, 2005].

[39] Geochemical studies indicate that fluids are released from the subducting crust and sediments in the region where tremor and slow slip are observed [e.g., *Peacock, 1993; Hyndman and Peacock, 2003*]. These same geochemical studies also indicate that the introduction of fluids to the overlying mantle in this region is likely fracture-controlled and eventually interacts with the overlying mantle peridotite to form serpentinite, reducing the density and seismic velocity and increasing Poisson's ratio of the overlying mantle [*Hyndman and Peacock, 2003; Christensen, 2004; Evans, 2004*]. Field evidence shows that fluid movement and serpentinization in the mantle is likely fracture controlled [*Evans, 2004*]. These material changes are corroborated in Cascadia by seismic studies that indicate anomalously low shear wave velocities in the overlying mantle [e.g., *Bostock et al., 2002; Brocher et al., 2003; Nicholson et al., 2005*]. Magnetotelluric studies in Japan [*Seno et al., 2001; Matsumoto et al., 2003; Umeda et al., 2006*] and Cascadia [*Kurtz et al., 1986; Soyer and Unsworth, 2006*] show conductivity anomalies in the lower crust above the subducting slab that are interpreted to result from the presence of interconnected fluids. In Cascadia the anomaly is located at approximately 20 km beneath Vancouver Island [*Soyer and Unsworth, 2006*].

4.3. Discussion and Source Hypotheses

[40] Choice of a definitive model from plausible models for tremor depends critically on which of the depth distributions of tremor reported in the many existing studies is the correct one. Three location methods in Cascadia [*McCausland et al. [2005], Kao et al. [2006]*, and this experiment] have found that the tremor locations have a depth distribution that is different than simply locating along the modeled subduction zone interface. Other studies in Cascadia and in Japan have found that some fraction of the signal can be explained by low frequency earthquakes that locate on or very near the modeled subducting plate interface, and these studies suggest that these signals interfere in such a way as to produce the near continuous recorded displacements [*Rogers and Dragert, 2003; Shelly et al., 2006; La Rocca et al., 2009*]. The three methods that find a larger depth distribution make no assumption about the nature of the tremor source. Furthermore they use more of the wavefield, including the parts that cannot be explained by low frequency earthquakes, while allowing for the inclusion of low frequency earthquakes within the tremor signal. In the following paragraphs, we consider two possible models for tremor source location and the relevant supporting observations for each. In the first model, the tremor signal is comprised only of the collective radiation from low frequency earthquakes located only on the subduction interface, and is consistent with the depth distribution in Japan of *Shelly et al. [2006]*. In a second model, the tremor signal is more broadly distributed in location (both at and near the subducting slab interface), is comprised in part by low-frequency earthquakes, but is triggered by stress and fluid pressure changes caused by slow slip.

[41] It is important to note that many properties of tectonic tremor are consistent with both source models, such as the coincidence of tremor with slow slip events, the slow migration of tremor epicenters roughly coincident with the migration of slow slip events, the long duration and emer-

gent onset of the signals, the dominance of SH waves in the tremor wavefield, and the presence of P and S wave pairs in the signals [*La Rocca et al., 2005, 2009, 2010*]. Both models are consistent with the geochemical and geophysical constraints on the presence of confined, pressurized fluids throughout a volume above the slab. An increase in fluid pressure results in a decrease in effective normal stress on fractures allowing for strain energy release at low shear stresses. These resulting strain releases (e.g., low stress drop earthquakes) need not be limited to the subduction interface. The fault slip may be reasonably as broad as the source region of the dehydration and mantle hydration reactions, consisting of a distributed set of pressurized faults and fractures. There are several examples of the phenomenon of fluid-reduced normal stresses and subsequent failure in other tectonic settings [e.g., *Vidale and Shearer, 2006; Segall et al., 2006*]. The presence of confined fluids can explain the concurrence of tremor and slow slip events both if the coincidence of tremor and slow slip are manifestations of the same phenomenon at different source time scales, and if the occurrence of the slow slip event changes the stress in the surrounding material, which in turn increases pore pressure and allows localized low frequency earthquakes.

[42] Several of the findings from this experiment are also consistent with both models. First are the short-term (minutes to hours) migration patterns of the tremor, where the tremor sometimes jumps from one region to another in any direction. This implies that the slow slip and tremor are not the simple unzipping or smooth propagation of a rupture front. Furthermore the tremor epicenter volume migrates both away and toward the trench within hours at the same point along strike of the subduction zone, and within a given volume the epicenters have no specific migration pattern, both of which are more similar to a tectonic aftershock distribution or swarm than a propagating rupture front. Perhaps the tectonic tremor and slow slip process is a very slow version of an earthquake, where in large-scale (for tremor, this is days) the tremor migrates smoothly along strike; but in fine-scale (minutes to days), the rupture is complicated and possibly linked to more than one asperity along the fault plane or planes, like for the rupture fronts modeled for the 2004 Parkfield earthquake [e.g., *Ma et al., 2008*] and 2004 Sumatra earthquake [*Ishii et al., 2005*].

[43] Because studies of tremor location relative to the subducting slab interface are not in agreement, we must consider the possibility that the depth locations in our study or in other studies are in error. Most of the studies to date in Cascadia find the sources to be distributed [*McCausland et al., 2005; Kao et al., 2007*], but new techniques are being developed and larger arrays are being deployed, and results from these studies shows evidence of low frequency events within the tremor that concentrate closer to the subduction interface [*La Rocca et al., 2009, 2010*]. Therefore consider first that the depth distribution in the current study is an artifact of the processing methods or velocity models used, and that the tremor signal is indeed comprised only of the collective radiation from many low frequency earthquakes on the subducting plate interface. These low frequency earthquakes could represent the release of seismic energy in the transition zone, between stick-slip and stable sliding behavior. We know that their low frequency content is a product of the source process because regional earthquakes

of similar depths have a normal tectonic earthquake spectrum. The low frequency content is compatible with low-stress drop earthquakes that occur in a material with a very low shear modulus [e.g., *Kamaya et al.*, 2004; *Ito and Obara*, 2006a, 2006b]. The juxtaposition of broadband tectonic events and tectonic tremor would suggest that the material properties at these depths are spatially heterogeneous and when the strain rates are high, broadband earthquakes are produced. But in areas with a low shear modulus and when the strain rate is low (and close to static), low frequency earthquakes are produced. This model, where the tremor is composed of low frequency events located on the interface in studies to date, presumes the plate interface is a well-defined, single fault zone; however geodetic models cannot rule out the possibility that the slow slip source is on a distributed in a thicker shear zone or wedge, or that the slip is occurring on portions of the slab that have delaminated from the downgoing plate, as reflectors delineated by seismic reflection data under Vancouver Island could be interpreted [*Nicholson et al.*, 2005]. The low frequency earthquake locations in Cascadia [*La Rocca et al.* 2009, 2010] have better resolution than the current experiment because one can identify both P and S wave phases or S-P times within the tremor signal. However, it has yet to be demonstrated at a high level of certainty that the entire tremor wavefield is made up of these low frequency earthquakes.

[44] Now consider that the depth distribution of the tremor locations in this study is real, that the tremor is partly comprised of low frequency earthquakes that occur along the downgoing slab interface, but that some fraction of the tremor signal results from sources that locate above or below that interface. This model assumes that the tremor signal results from slip or rapid motion at high fluid pressures in confined faults and fractures, with off-slab high fluid pressures generated by local changes in the stress field around the slab interface during a slow slip event. The off-slab signals could be low frequency earthquakes or another seismic process that lacks clear P and S wave phases on structures parallel or perpendicular to the plate interface. Consider as well that off-slab signals could occur because the slab interface is not a single well-defined plane but rather a distributed wider shear zone, including the occurrence of tremor and slip on portions of the subducting slab that have delaminated. Instead of being confined to a well-defined fault plane, the tremor occurs at depths that reflect the structure of the shear zone and stress field.

[45] The events making up the tremor are essentially continuous (identified on one array (Lopez) during 99% of the 2004 tectonic tremor and slow slip episode), and the tremor episodes have small variations in maximum amplitudes within and between episodes [*McCausland et al.*, 2005], indicating that the tremor does not obey the same magnitude scaling relationship as tectonic earthquakes. In fact they exhibit characteristics more akin to earthquake swarms than main shock-aftershock sequences. This model allows the material properties to vary over short distances in all directions, whereby the low frequency earthquakes are occurring in material that is more brittle and the slip is occurring in material that is more ductile. This variation in material properties explains how broadband tectonic earthquakes can be located in the same areas as the tectonic tremor and slow slip events. Results described in this paper and

previous network results of source location, which show a wide depth distribution, are consistent with the second source model.

5. Conclusions

[46] This experiment was the first to use small aperture seismic arrays to track the location of tectonic tremor using a time-windowing approach. Our purpose in determining the spatial and temporal evolution of tremor during large tectonic tremor and slow slip episode is to better constrain possible physical mechanisms of tremor and how it relates to subduction zone structure and therefore to regional seismic hazard in northern Cascadia. To study the July 2004 Cascadia tectonic tremor and slow slip episode, we used three small aperture seismic arrays above the subduction zone with locations chosen to surround the initiation point of several previous tectonic tremor and slow slip episodes. Using 5 min duration windows, we found that tectonic tremor was active up to 99 percent of the tremor and slow slip episode, a result that suggests that network derived tremor counts are greatly underestimated.

[47] Tectonic tremor locations were calculated by tracking individual wave phases across the stations of the arrays and comparing those vectors to ones derived using standard layered Earth velocity model. Uncertainties in the best locations are 5 km in epicenter and 16 km depth. At the beginning of the episode when the locations are best resolved, the tectonic tremor locations were found to be stationary within a volume roughly 250 km in epicenter and 20 km in depth for hours to days before moving to a new volume; the movement of the tremor locations within a given volume followed no specific pattern. The transition between volumes was not a smooth unidirectional migration; rather the locations begin to transition, return to the original volume and restart the transition. We observed transitions in both the updip and downdip directions. The overall daily migration speeds estimated from the data agree with previous studies, but small scale (minutes) estimates of the source migration speeds yielded values as fast as 2 km/min, a detail that cannot be determined from network data.

[48] We considered our results and those of previous studies of tectonic tremor and slow slip in Cascadia and existing constraints from geophysics, seismology and geochemistry of the region to address possible physical mechanisms responsible for tremor. We argue that the collective evidence suggests, but does not definitively require, that tectonic tremor is related to the presence of fluids at depth, but whether the presence of fluids causes the tremor and slow slip or just facilitates their occurrence under the correct stress conditions is not yet clear. Our favored model is that pressurized pore fluids reduce normal stresses along pre-existing faults and fractures at and near the subducting plate interface causing low stress drop earthquakes that make up at least part of the tremor signal, and that the migration of tremor is not a smooth process indicating variability in slab conditions material properties at the locations of the tremor sources along dip and strike of the Cascadia subduction zone.

[49] In Cascadia, it remains unclear whether tremor is concentrated on the subduction interface or is more distributed; our results suggest that it is distributed. To distinguish between interface and distributed models of tectonic

tremor source, some issues must be resolved and additional data acquired. For example, the location and configuration of the slab interface is not known precisely. Studies that have modeled the slab interface are based primarily on velocity changes (reflection surveys), earthquake locations, and receiver functions; thus, we cannot truly know if the tremor is locating on the subducting slab interface, on a series of planes that define the interface, within the plate, or just above. Further data relating the exact timing of the initiation of the tremor and slip events is required to understand which occurs first and if they always accompany one another. Studies using the Plate Boundary Observatory borehole strainmeters can resolve slow events on shorter time scales than with GPS data. Using the co-located borehole seismometers, which have better signal-to-noise than surface stations, one also might discern the relative timing of the initiation of slow slip events and tremor.

[50] **Acknowledgments.** The Deep Tremor Project 2004 was funded by NSF EAR-0337144. Seismic sensors used at Lopez and Sequim array were financed and loaned by AMRA, Regione Campania, Italy. Seismic stations used at Sooke were provided by the PASSCAL instrument pool of IRIS. The authors gratefully acknowledge the assistance of personnel from the Pacific Northwest Seismograph Network and from the Pacific Geoscience Centre who provided valuable discussions and assisted in the installation and servicing of the Sooke array. We also thank E. Roeloffs, Nick Beeler, the reviewers, and editors for their comments that improved the quality of this paper.

References

- Aster, R., B. Borchers, and C. Thurber (2004), *Parameter Estimation and Inverse Problems*, Elsevier Sci. and Technol., Burlington, Mass.
- Bostock, M. G., R. D. Hyndman, S. Rondenay, and S. M. Peacock (2002), An inverted continental Moho and serpentinization of the forearc mantle, *Nature*, *417*, 536–538, doi:10.1038/417536a.
- Brocher, T. M., T. Parsons, A. M. Trehu, C. M. Snelson, and M. A. Fisher (2003), Seismic evidence for widespread serpentinized forearc upper mantle along the Cascadia margin, *Geology*, *31*(3), 267–270, doi:10.1130/0091-7613(2003)031<0267:SEFWFS>2.0.CO;2.
- Brooks, B., J. H. Foster, M. Bevis, L. N. Frazer, C. J. Wolfe, and M. B. Behn (2006), Periodic slow earthquakes on the flank of Kilauea volcano, Hawaii, *Earth Planet. Sci. Lett.*, *246*, 207–216, doi:10.1016/j.epsl.2006.03.035.
- Christensen, N. I. (2004), Serpentinites, peridotites, and seismology, in *Serpentine and Serpentinites: Mineralogy, Petrology, Geochemistry, Ecology, Geophysics and Tectonics*, edited by W. G. Ernst, pp. 503–524, Bellwether, Columbia, Md.
- Crosson, R. S. (1976), Crustal structure modeling of earthquake data 1. Simultaneous least squares estimation of hypocenter and velocity parameters, *J. Geophys. Res.*, *81*(17), 3036–3046, doi:10.1029/JB081i017p03036.
- Crotwell, H. P., T. J. Owens, and J. Ritsema (1999), The TauP Toolkit: Flexible seismic travel-time and ray-path utilities, *Seismol. Res. Lett.*, *70*, 154–160.
- Douglas, A., J. Beavan, L. Wallace, and J. Townend (2005), Slow slip on the northern Hikurangi subduction interface, New Zealand, *Geophys. Res. Lett.*, *32*, L16305, doi:10.1029/2005GL023607.
- Dragert, H., K. Wang, and T. S. James (2001), A silent slip event on the deeper Cascadia Subduction Interface, *Science*, *292*, 1525–1528, doi:10.1126/science.1060152.
- Evans, B. (2004), The serpentinite multi-system revisited: Chrysotile is metastable, in *Serpentine and Serpentinites: Mineralogy, Petrology, Geochemistry, Ecology, Geophysics and Tectonics*, edited by W. G. Ernst, pp. 5–32, Bellwether, Columbia, Md.
- Hirose, H., and K. Obara (2005), Repeating short- and long-term slow slip events with deep tremor activity around the Bungo channel region, southwest Japan, *Earth Planets Space*, *57*, 961–972.
- Hyndman, R., and S. M. Peacock (2003), Serpentinization of the forearc mantle, *Earth Planet. Sci. Lett.*, *212*, 417–432, doi:10.1016/S0012-821X(03)00263-2.
- Ishii, M., P. M. Shearer, H. Houston, and J. E. Vidale (2005), Extent, duration and speed of the 2004 Sumatra–Andaman earthquake imaged by the Hi-Net array, *Nature*, *435*, 933–936, doi:10.1038/nature03675.
- Ito, Y., and K. Obara (2006a), Dynamic deformation of the accretionary prism excites very low frequency earthquakes, *Geophys. Res. Lett.*, *33*, L02311, doi:10.1029/2005GL025270.
- Ito, Y., and K. Obara (2006b), Very low frequency earthquakes within accretionary prisms are very low stress-drop earthquakes, *Geophys. Res. Lett.*, *33*, L09302, doi:10.1029/2006GL025883.
- Ito, Y., K. Obara, K. Shiomi, S. Sekine, and H. Hirose (2007), Slow earthquakes coincident with episodic tremors and slow slip event, *Science*, *315*(5811), 503, doi:10.1126/science.1134454.
- Kamaya, N., A. Katsumata, and Y. Ishigaki (2004), Low-frequency tremor and slow slip around the probably source region of the Tokai earthquake—A new indicator for the Tokai earthquake prediction provided by unified seismic networks in Japan, *U.S. Geol. Surv. Open File Rep.*, *2005-1131*, 47 pp.
- Kao, H., and S. Shan (2004), The source-scanning algorithm: Mapping the distribution of seismic sources in time and space, *Geophys. J. Int.*, *157*(2), 589–594, doi:10.1111/j.1365-246X.2004.02276.x.
- Kao, H., S. Shan, H. Dragert, G. Rogers, J. F. Cassidy, K. Wang, T. S. James, and K. Ramachandran (2005), A wide depth distribution of seismic tremors along the northern Cascadia margin, *Nature*, *436*(7052), 841–844, doi:10.1038/nature03903.
- Kao, H., S. Shan, H. Dragert, G. Rogers, J. F. Cassidy, K. Wang, T. S. James, and K. Ramachandran (2006), Spatial-temporal patterns of seismic tremors in northern Cascadia, *J. Geophys. Res.*, *111*, B03309, doi:10.1029/2005JB003727.
- Kao, H., S. -J. Shan, G. Rogers, and H. Dragert (2007), Migration characteristics of seismic tremors in the northern Cascadia margin, *Geophys. Res. Lett.*, *34*, L03304, doi:10.1029/2006GL028430.
- Kurtz, R. D., J. M. DeLaurier, and J. C. Gupta (1986), A magnetotelluric sounding across Vancouver Island detects the subducting Juan de Fuca plate, *Nature*, *321*, 596–599, doi:10.1038/321596a0.
- La Rocca, M., W. McCausland, D. Galluzzo, S. Malone, G. Saccorotti, and E. Del Pezzo (2005), Array measurements of deep tremor signals in the Cascadia subduction zone, *Geophys. Res. Lett.*, *32*, L21319, doi:10.1029/2005GL023974.
- La Rocca, M., D. Galluzzo, S. Malone, W. McCausland, G. Saccorotti, and E. Del Pezzo (2008), Testing small-aperture array analysis on well-located earthquakes, and application to the location of deep tremor, *Bull. Seismol. Soc. Am.*, *98*, 620–635, doi:10.1785/0120060185.
- La Rocca, M., K. C. Creager, D. Galluzzo, S. Malone, J. E. Vidale, J. R. Sweet, and A. G. Wech (2009), Cascadia tremor located near plate interface constrained by S minus P wave times, *Science*, *323*, 620–623, doi:10.1126/science.1167112.
- La Rocca, M., D. Galluzzo, S. Malone, W. McCausland, and E. Del Pezzo (2010), Array analysis and precise source location of deep tremor in Cascadia, *J. Geophys. Res.*, *115*, B00A20, doi:10.1029/2008JB006041.
- Ma, S., S. Custódio, R. J. Archuleta, and P. Liu (2008), Dynamic modeling of the 2004 Mw6.0 Parkfield, California, earthquake, *J. Geophys. Res.*, *113*, B02301, doi:10.1029/2007JB005216.
- Matsumoto, T., T. Kawabata, J. Matsuda, K. Yamamoto, and K. Mimura (2003), 3He/4He ratios in well gases in the Kinki district, SW Japan: Surface appearance of slab-derived fluids in a non-volcanic area in Kii Peninsula, *Earth Planet. Sci. Lett.*, *216*(1–2), 221–230, doi:10.1016/S0012-821X(03)00479-5.
- McCausland, W. (2006), Tracking subduction tremor in Cascadia using regional network and small aperture seismic array data, Ph.D. dissertation, Univ. of Wash., Seattle.
- McCausland, W., S. Malone, and D. Johnson (2005), Temporal and spatial occurrence of deep non-volcanic tremor: From Washington to northern California, *Geophys. Res. Lett.*, *32*, L24311, doi:10.1029/2005GL024349.
- Medema, G. F. (2006), Juan de Fuca subducting plate geometry and intra-slab seismicity, doctoral dissertation, Univ. of Wash., Seattle.
- Miller, M., T. Melbourne, D. J. Johnson, and W. Q. Sumner (2002), Periodic slow earthquakes from the Cascadia subduction zone, *Science*, *295*, 2423, doi:10.1126/science.1071193.
- Nadeau, R. M., and D. Dolenc (2005), Nonvolcanic tremors deep beneath the San Andreas fault, *Science*, *307*, 389, doi:10.1126/science.1107142.
- Nicholson, T., M. Bostock, and J. F. Cassidy (2005), New constraints on subduction zone structure in northern Cascadia, *Geophys. J. Int.*, *161*, 849–859, doi:10.1111/j.1365-246X.2005.02605.x.
- Obara, K. (2002), Non-volcanic deep tremor associated with subduction in southwest Japan, *Science*, *296*, 1679–1681, doi:10.1126/science.1070378.

- Peacock, S. M. (1993), Large-scale hydration of the lithosphere above subducting slabs, *Chem. Geol.*, *108*, 49–59, doi:10.1016/0009-2541(93)90317-C.
- Preston, L., K. C. Creager, R. S. Crosson, T. M. Brocher, and A. M. Trehu (2003), Intraslab earthquakes: Dehydration of the Cascadia slab, *Science*, *302*, 1197–1200, doi:10.1126/science.1090751.
- Rogers, G., and H. Dragert (2003), Episodic tremor and slip on the Cascadia subduction zone: The chatter of silent slip, *Science*, *300*, 1942–1943, doi:10.1126/science.1084783.
- Schwartz, S. Y., and J. M. Rokosky (2007), Slow slip events and seismic tremor at circum-Pacific subduction zones, *Rev. Geophys.*, *45*, RG3004, doi:10.1029/2006RG000208.
- Segall, P., E. K. Desmarais, D. Shelly, A. Miklius, and P. Cervelli (2006), Earthquakes triggered by silent slip events on Kilauea volcano, *Hawaii, Nature*, *442*, 71–74, doi:10.1038/nature04938.
- Seno, T., D. Zhao, Y. Kobayashi, and M. Nakamura (2001), Dehydration of serpentinized slab mantle: Seismic evidence from southwest Japan, *Earth Planets Space*, *53*, 861–871.
- Shelly, D. R., G. C. Beroza, S. Ide, and S. Nakamura (2006), Low-Frequency Earthquakes in Shikoku, Japan, and their relationship to episodic tremor and slip, *Nature*, *442*, 188–191, doi:10.1038/nature04931.
- Shelly, D. R., G. C. Beroza, and S. Ide (2007), Complex evolution of transient slip derived from precise tremor locations in western Shikoku, Japan, *Geochem. Geophys. Geosyst.*, *8*, Q10014, doi:10.1029/2007GC001640.
- Soyer, W., and M. Unsworth (2006), Deep electrical structure of the northern Cascadia (British Columbia, Canada) subduction zone: Implications for the distribution of fluids, *Geology*, *34*, 53–56, doi:10.1130/G21951.1.
- Szeliga, W., T. I. Melbourne, M. M. Miller, and V. M. Santillan (2004), Southern Cascadia episodic slow earthquakes, *Geophys. Res. Lett.*, *31*, L16602, doi:10.1029/2004GL020824.
- Umeda, K., Y. Ogawab, K. Asamoria, and T. Oikawaa (2006), Aqueous fluids derived from a subducting slab: Observed high ³He emanation and conductive anomaly in a non-volcanic region, Kii Peninsula southwest Japan, *J. Volcanol. Geotherm. Res.*, *149*, 47–61, doi:10.1016/j.jvolgeores.2005.06.005.
- Vidale, J. E., and P. M. Shearer (2006), A survey of 71 earthquake bursts across southern California: Exploring the role of pore fluid pressure fluctuations and aseismic slip as drivers, *J. Geophys. Res.*, *111*, B05312, doi:10.1029/2005JB004034.
- Wallace, L. M., and J. Beavan (2006), A large slow slip event on the central Hikurangi subduction interface beneath the Manawatu region, North Island, New Zealand, *Geophys. Res. Lett.*, *33*, L11301, doi:10.1029/2006GL026009.
- Wech, A. G., and K. C. Creager (2007), Cascadia tremor polarization evidence for plate interface slip, *Geophys. Res. Lett.*, *34*, L22306, doi:10.1029/2007GL031167.

K. C. Creager and S. D. Malone, Department of Earth and Space Sciences, University of Washington, Box 35130, Seattle, WA 98195, USA.
 M. La Rocca, Istituto Nazionale di Geofisica e Vulcanologia, Osservatorio Vesuviano, Via Diocleziano, 328, I-80124 Napoli, Italy.
 W. A. McCausland, U.S. Geological Survey, Cascades Volcano Observatory, 1300 SE Cardinal Ct., Bldg. 10, Ste. 100, Vancouver, WA 98683, USA. (wmccausland@usgs.gov)